Copernicus FRM4SOC FICE 2025

Training on
In Situ Ocean Colour Radiometry

Introduction to above-water radiometry

Giuseppe Zibordi

giuseppe.zibordi@eoscience.eu

PROGRAMME OF THE EUROPEAN UNION
Copernicus Europe's eyes on Earth
IMPLEMENTED BY EUMETSAT
FRM4SOC Phase-2
fiducial reference measurements for satellite ocean colour
CNR ISMAR ISTITUTO DI SCIENZE MARINE

7-19 July 2025
Venice, Italy

Valuable sentences

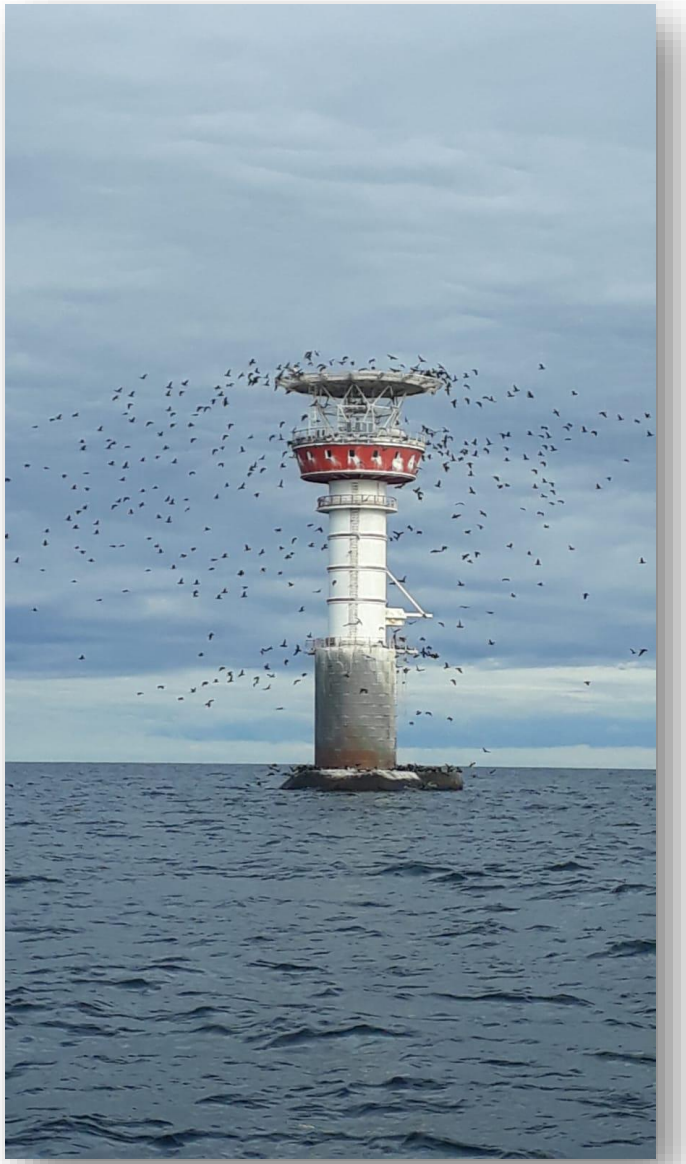

'Good (practically useful) data do not collect themselves. Neither do they magically appear on one's desk, ready for analysis and lending insight into how to improve processes' (Vardemann and Jobe 2016)

'… adequately sampled, carefully calibrated, quality controlled, and archived data for key elements of the climate system will be useful indefinitely' (Wunsch et al. 2013)

'… a measurement of any kind is incomplete unless accompanied with an estimate of the uncertainty associated with that measurement ' (Palmer and Grant, 2010)

'… we should do the radiometry correctly, or not do it at all' (Richard Beck, 2022)

Validation of satellite data products

Validation is the process of assessing, by independent means, the quality of the data products derived from the system outputs

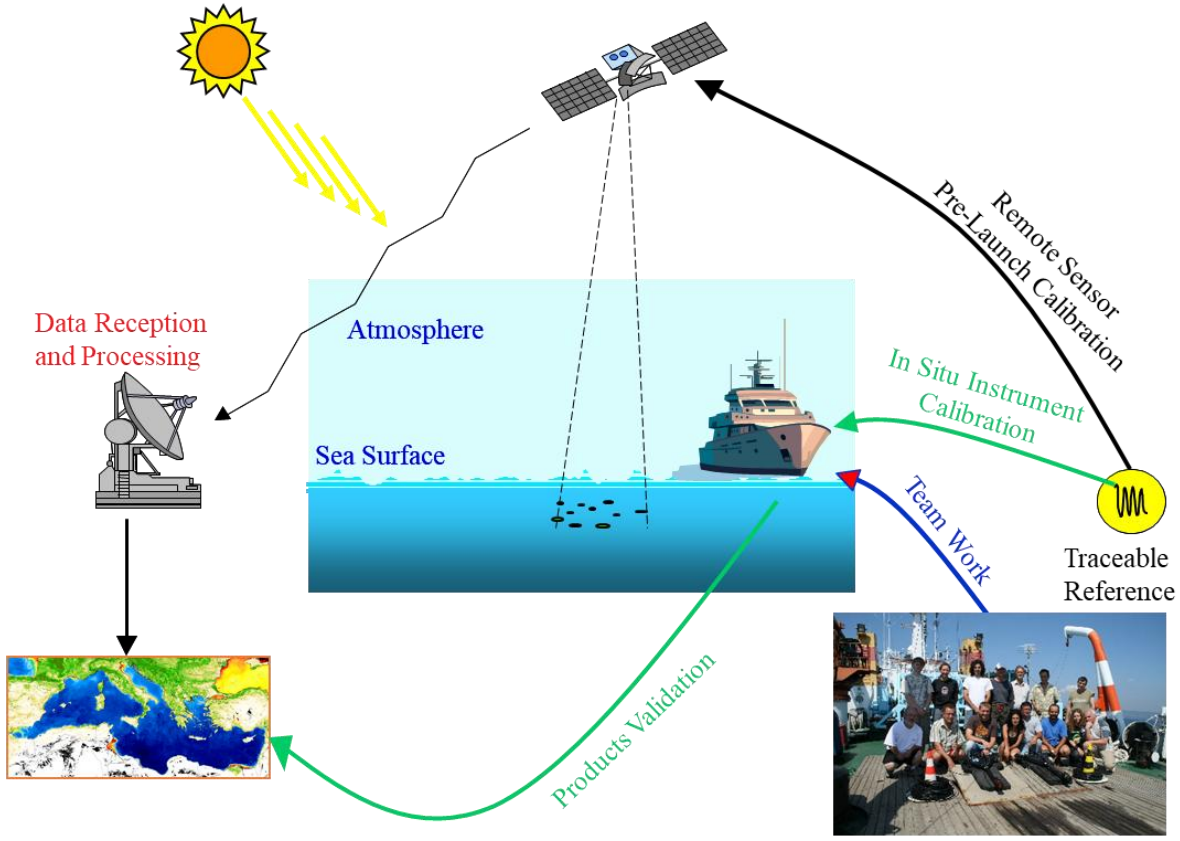

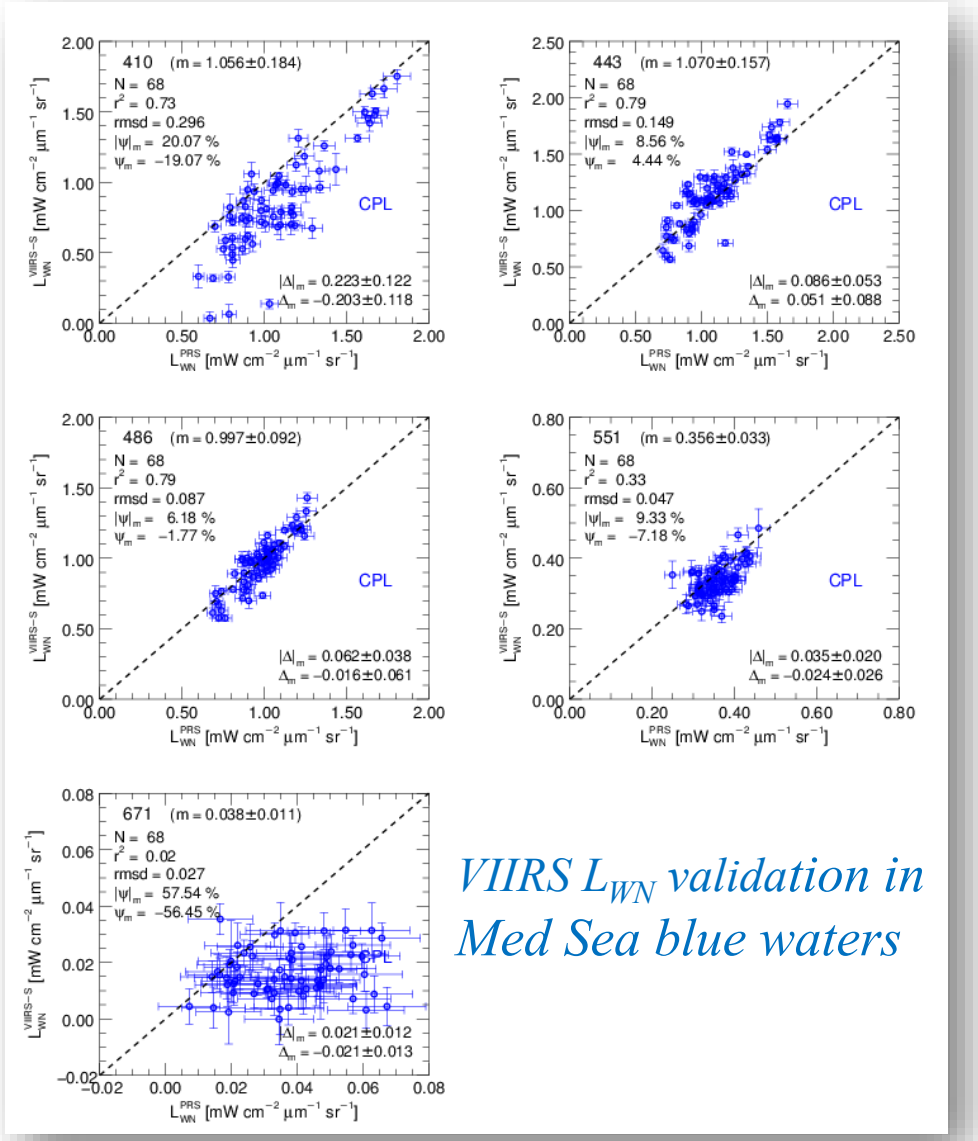

VIIRS L_{WN} validation in Med Sea blue waters

Spectral irradiance

The spectral plane irradiance is a measure of the flux per unit surface area and wavelength. This quantity, commonly expressed in $W\ m^{-2}\ nm^{-1}$, is measured through a horizontal collector exhibiting cosine angular response.

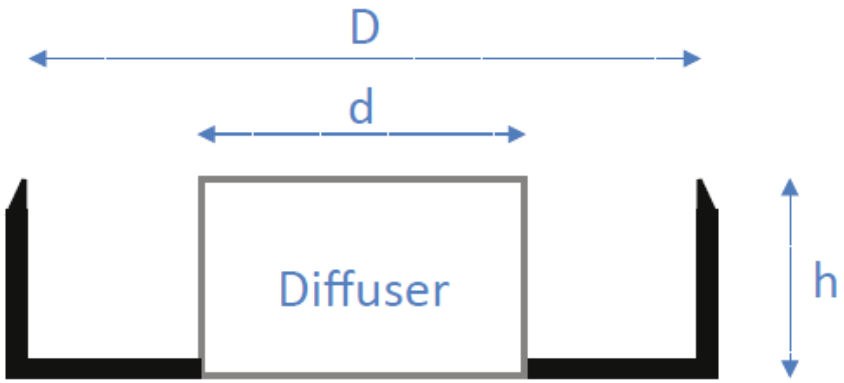

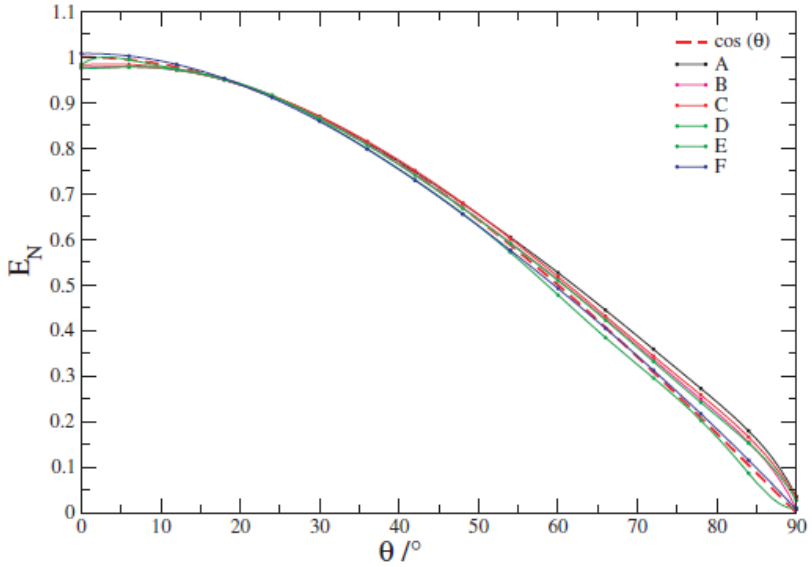

The accuracy of the cosine response and its stability over time, are fundamental elements of any plane irradiance sensor.

Irradiance collectors are specifically designed for in-air or alternatively for in-water applications.

A plane irradiance of relevance for above-water radiometry is the downward spectral irradiance $E_s(\lambda)$ quantified above the water surface.

Spectral radiance

Spectral radiance is a measure of the flux per unit solid angle, unit projected area and wavelength. This is a directional quantity commonly measured in $W\ sr^{-1}\ m^{-2}\ nm^{-1}$ through a conical field-of-view.

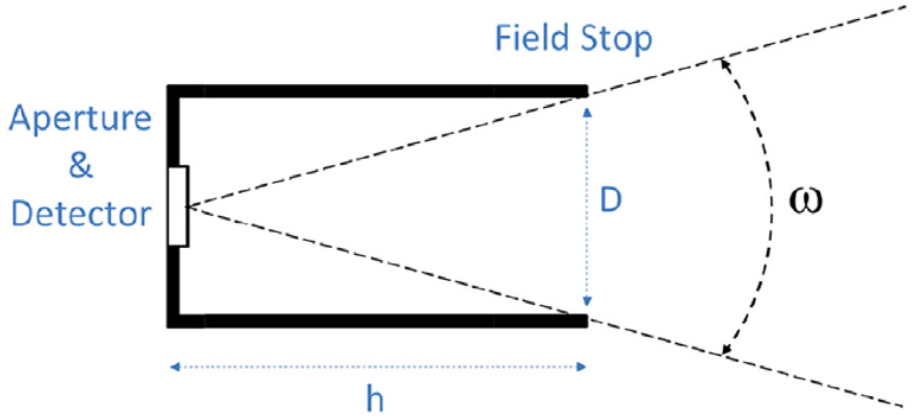

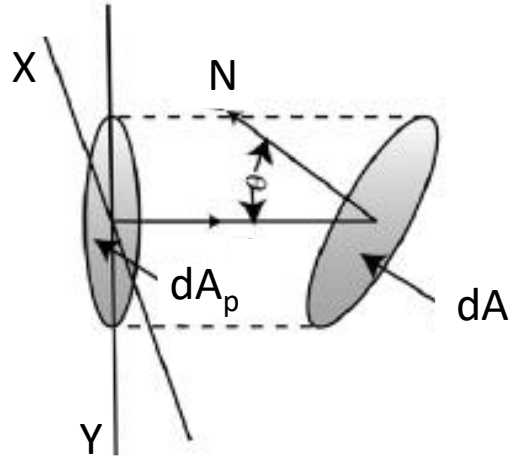

A basic assumption underlying radiance measurements is the spatial homogeneity of the flux in the sensor full-angle field-of-view.

Assuming a full-angle field-of-view ω, the related solid angle is $\Omega = 2\pi\cdot(1-\cos(\omega / 2))$.

The most common ocean colour radiance quantity is the spectral water-leaving radiance $L_w(\lambda)$, which is the radiance emerging from below the water surface, quantified just above the surface and carrying information on the absorption and scattering properties of the optically significant water constituents as a function of wavelength λ.

Terminology

$L_w(0^+)$ –> water-leaving radiance (above water)

$E_d(0^+)$ –> downward irradiance (often indicated as E_s)

$L_{wn}(0^+)$ –> normalized water-leaving radiance ($L_w(0^+)$/ $E_d(0^+)$*E_0)

$R_{rs}(0^+)$ –> remote sensing reflectance ($L_w(0^+)$/ $E_d(0^+)$)

$L_{WN}(0^+)$ –> exact $L_{wn}(0^+)$ ($L_{wn}(0^+)$ *brdf* corrected)

$R_{RS}(0^+)$ –> exact $R_{rs}(0^+)$ (*i.e.*, $R_{rs}(0^+)$ *brdf* corrected)

Multispectral and Hyperspectral radiometers

Multispectral radiometers have a few spectral bands typically 10 nm wide commonly chosen to match those of satellite sensors.

Hyperspectral radiometers exhibit a number of spectral bands typically varying from tens to hundreds.

Hyperspectral →

Solar spectrum →

Multispectral →

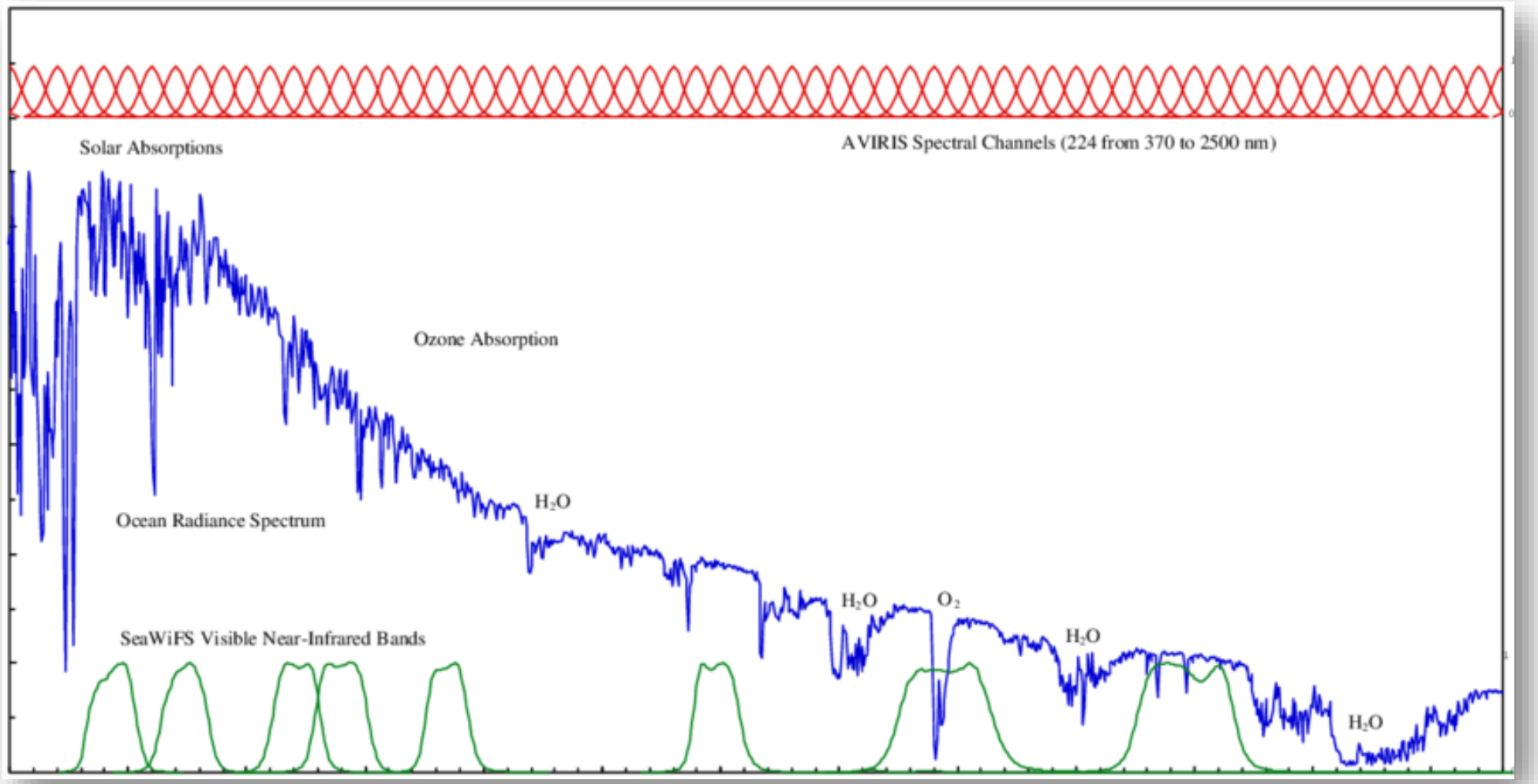

Multispectral vs Hyperspectral radiometers

The bands of *multi-spectral radiometers* rely on *spectral band-pass filters* coupled to photodetectors. Multispectral radiometers benefit of relatively simple optics design, which normally minimizes sensitivity to polarization and stray lights (light from one region of the spectrum interfering with light from another region). Still, the response outside the nominal band-passes (the so-called *out-of-band response*) may become the source of measurement errors depending on the spectral shape of the incoming light.

Hyperspectral radiometers rely on dispersive optical elements (*i.e., diffraction gratings or prisms*) to obtain spectral bands continuously distributed across the spectrum with resolution commonly comprised between 3 and 10 nm. The complexity of the optics due to various reflecting and diffracting components, make hyperspectral radiometers more affected by stray lights and sensitive to polarization and temperature, with effects varying with wavelength.

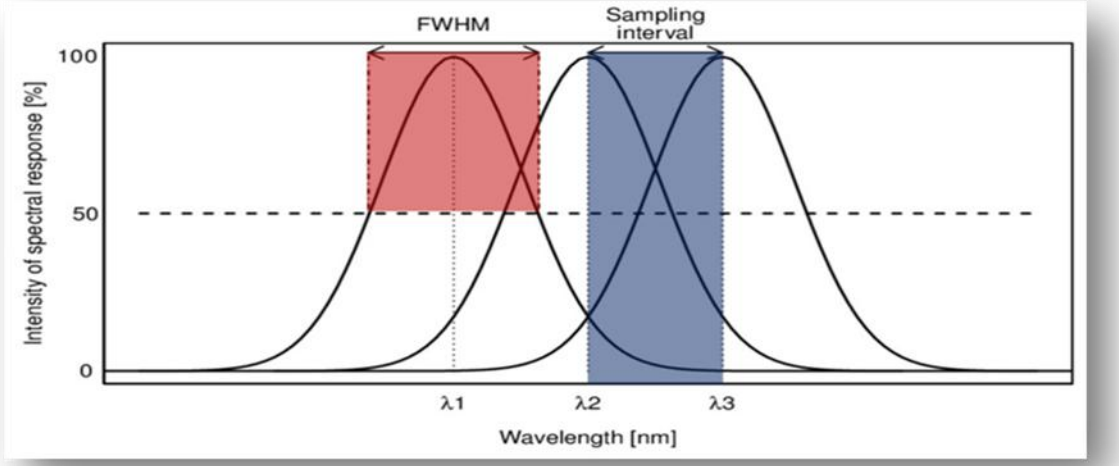

When evaluating the characteristics of hyperspectral radiometers, it is important to distinguish between the *spectral sampling* defining the distance between the center-wavelengths of contiguous bands, and the *spectral resolution* defining the amplitude of each band.

Tentative specifications for hyperspectral radiometers

Spectral Range:	380 to 900 nm (an extension in the ultraviolet is desirable)
Spectral Resolution:	3-10 nm (FWHM)
Spectral Sampling:	1-3 nm (or at least 1/2 the spectral resolution)
Wavelength Accuracy:	10 % FWHM resolution
Wavelength Stability:	5 % FWHM of resolution
Signal-to-Noise Ratio:	1000:1 (at minimum)
Stray Light Rejection:	10^{-5} (of the maximum radiometric signal at each spectral band)
FOV Maximum (full-angle):	5° (for above-water)
Temperature Stability:	Specified for 0–45°C
Linearity:	Correctable to 0.1 %

Absolute radiometric calibrations and characterizations confirming radiometers performance, require access to laboratory standards of spectral irradiance, reflectance plaques, spectral filters, regulated power supplies, … .

The standardization of radiometers through the adoption of a restricted number of instrument models targeting applications, would definitively make the characterization process more focused and consequently effective for the community.

IOCCG Protocol Series (2019). Protocols for Satellite Ocean Colour Data Validation: In Situ Optical Radiometry. Zibordi, G., Voss, K. J., Johnson, B. C. and Mueller, J. L. IOCCG Ocean Optics and Biogeochemistry Protocols for Satellite Ocean Colour Sensor Validation, Volume 3.0, IOCCG, Dartmouth, NS, Canada.

Quantitative radiometry

Fully recognizing all the efforts which generated know-how in marine optical radiometry beginning in the early 1920s, quantitative optical radiometry started in the mid 1960's thanks to development of spectral radiometers (Jerlov 1965, Tyler et al 1970) and the access to highly accurate secondary standards of spectral irradiance (Slater 1980).

DXW

1000-W FEL lamp introduced in 1975 as an improvement of the 1000-W DXW lamp from the mid-1960s

FEL

Major advances in the assessment and implementation of *in situ* marine optical radiometric measurement methods were driven by satellite ocean color missions.

The SeaWiFS program played a major role in such a development and assessment for more than a decade by supporting SIRREXs (e.g., Mueller 1992, Johnson et al. 1995, Johnson et al. 1999, Hooker et al. 2002, Zibordi et al. 2002) and finalizing the ocean optics protocols (*e.g.,* Mueller and Austin 1992, Mueller et al. 2003). ***The current IOCCG (2019) protocols are a follow up of those efforts.***

Above-water radiometry

Historical dates

1920s: First observations
1980s: Early documented method
1990s: Methods assessment
2000s: Comprehensive uncertainty analysis

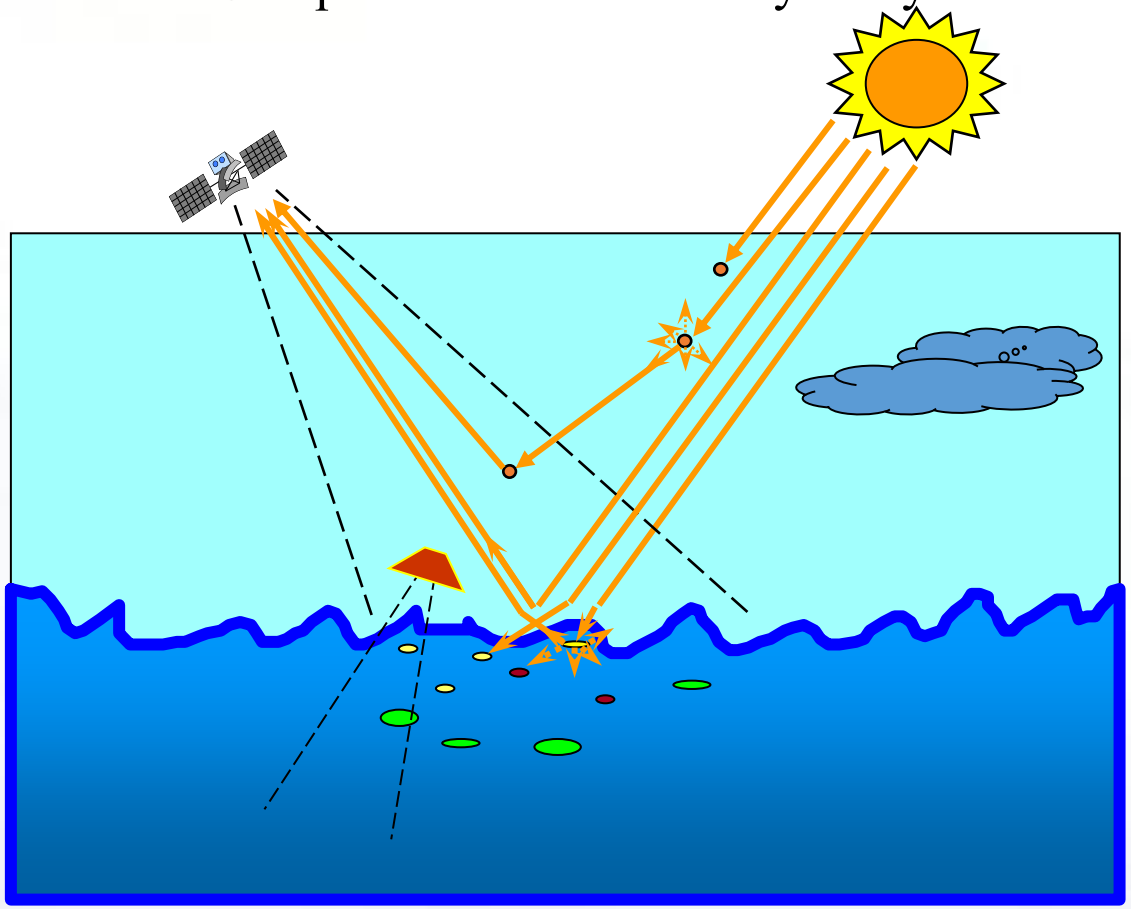

Advantages

1. Long-term deployments are insensitive to bio-fouling
2. Insensitive to coastal water optical stratifications

Drawbacks

1. Cannot produce profiles of radiometric quantities
2. Restricted to a few radiometric quantities (*i.e.*, L_w)
3. Requires correction for sea-surface reflected radiance contributions and non-nadir view
4. Highly sensitive to wave perturbations

Above-water radiometry

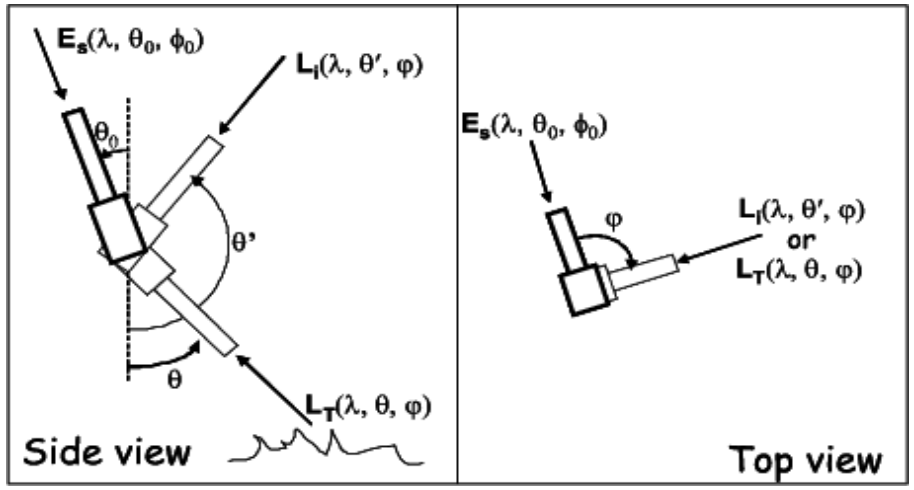

$$(\varphi = \varphi_0 + 90^0; \theta = 40^0; \theta' = 140^0)$$

Sky-radiance: L_i

Sea-radiance: L_T

$$L_W(\varphi, \theta, \lambda) = L_T(\varphi, \theta, \lambda) - \rho(\varphi, \theta, \theta_0, W) L_i(\varphi, \theta', \lambda)$$

$$L_W(\lambda) = L_W(\varphi, \theta, \lambda) C_{f/Q}(\lambda, \theta, \varphi, \theta_0, \tau_A, IOP, W)$$

$$L_{WN}(\lambda) = L_W(\lambda) \left(D^2 t_d(\lambda) \cos\theta_0\right)^{-1} C_{f/Q}(\lambda, \theta_0, \tau_A, IOP, W)$$

*

$E_0(\lambda) / E_d(0^+, \lambda)$

*

Morel, A. (1980). In-water and remote measurements of ocean color. Boundary-layer meteorology, 18(2), 177-201.

Carder, K. L., & Steward, R. G. (1985). A remote-sensing reflectance model of a red-tide dinoflagellate off west Florida 1. Limnology and oceanography, 30(2), 286-298.

Mobley, C. D. (1999). Estimation of the remote-sensing reflectance from above-surface measurements. Applied optics, 38(36), 7442-7455.

Zibordi, G., Hooker, S. B., Berthon, J. F., & D'Alimonte, D. (2002). Autonomous above-water radiance measurements from an offshore platform: a field assessment experiment. Journal of Atmospheric and Oceanic Technology, 19(5), 808-819.

Hooker, S. B., Lazin, G., Zibordi, G., & McLean, S. (2002). An evaluation of above-and in-water methods for determining water-leaving radiances. Journal of Atmospheric and Oceanic Technology, 19(4), 486-515.

The ρ-factor

ρ-factor –> sea surface reflectance factor (Mobley 1999),
–> radiance reflectance factor (Mobley 2015),
–> effective Fresnel reflect. coeff. (Ruddick et al. 2019),
–> surface-to-sky reflectance ratio (Harmel 2023).

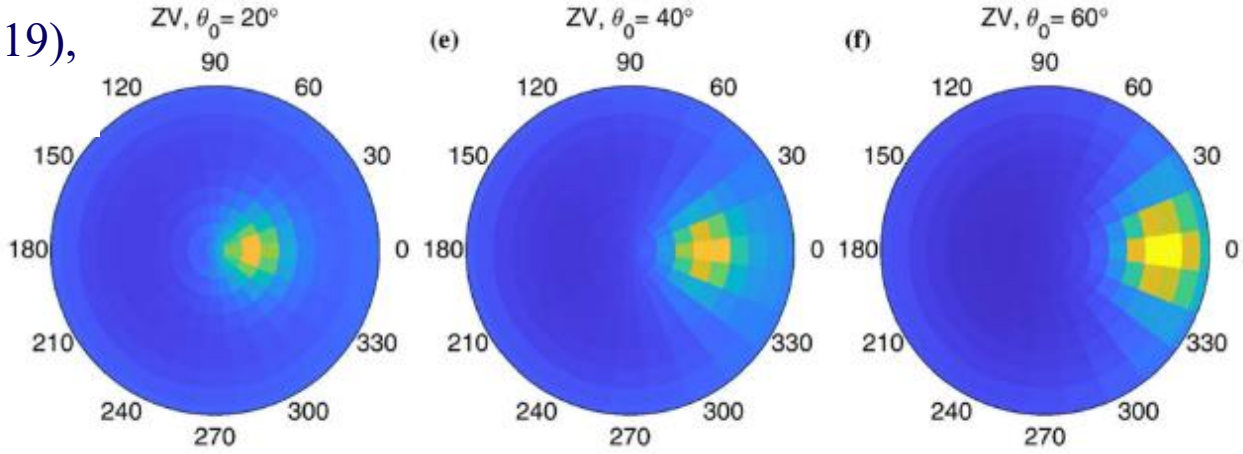

$L_{sky}(\theta, \phi)$

$$L_w(\theta,\phi,\lambda) = L_t(\theta,\phi,\lambda) - L_r(\theta,\phi,\lambda)$$

$$L_r(\theta,\phi) = \int_0^{2\pi}\int_0^{\frac{\pi}{2}} r(\theta^*,\phi^* \rightarrow \theta,\phi) L_{sky}(\theta^*,\phi^*) \sin\theta^* d\theta^* d\phi^*.$$

Sea surface reflectance function depending on Fresnel reflectance and wave statistics

$$L_r(\theta,\phi) = \rho L_i(\theta',\phi)$$

$$\rho = \frac{\int_0^{2\pi}\int_0^{\frac{\pi}{2}} r(\theta^*,\phi^* \rightarrow \theta,\phi) L_{sky}(\theta^*,\phi^*) \sin\theta^* d\theta^* d\phi^*}{L_i(\theta',\phi)}$$

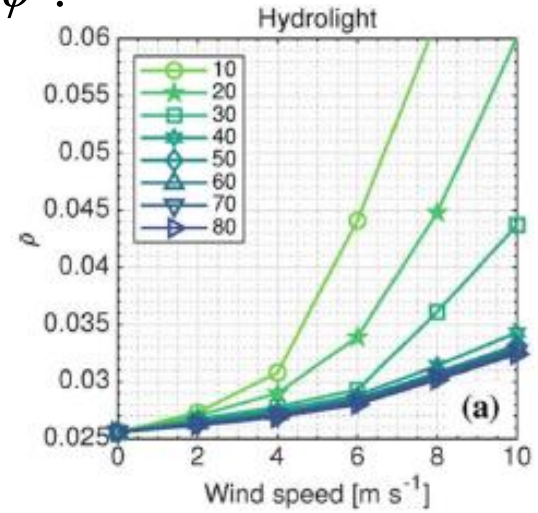

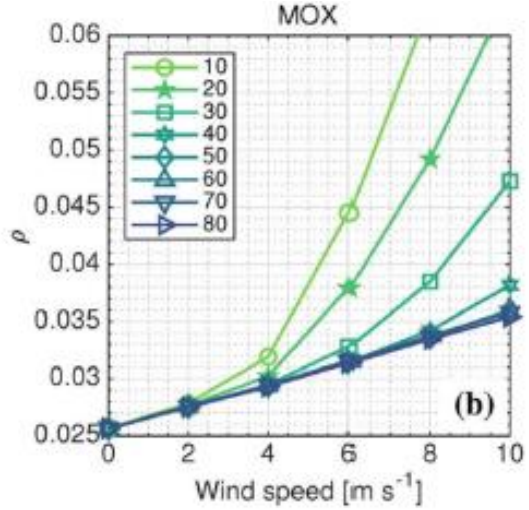

D'Alimonte, D., Kajiyama, T., Zibordi, G., & Bulgarelli, B. (2021). Sea-surface reflectance factor: replicability of computed values. Opt. Express, 29(16), 25217-25241.

Viewing geometry

Assuming a viewing angle θ=40°, the relative azimuth angle with respect to the sun is illustrated for ϕ=90° → and ϕ =135° →

This suggests a lower dependence of ϕ =135° on sea state expressed as a function of wind speed

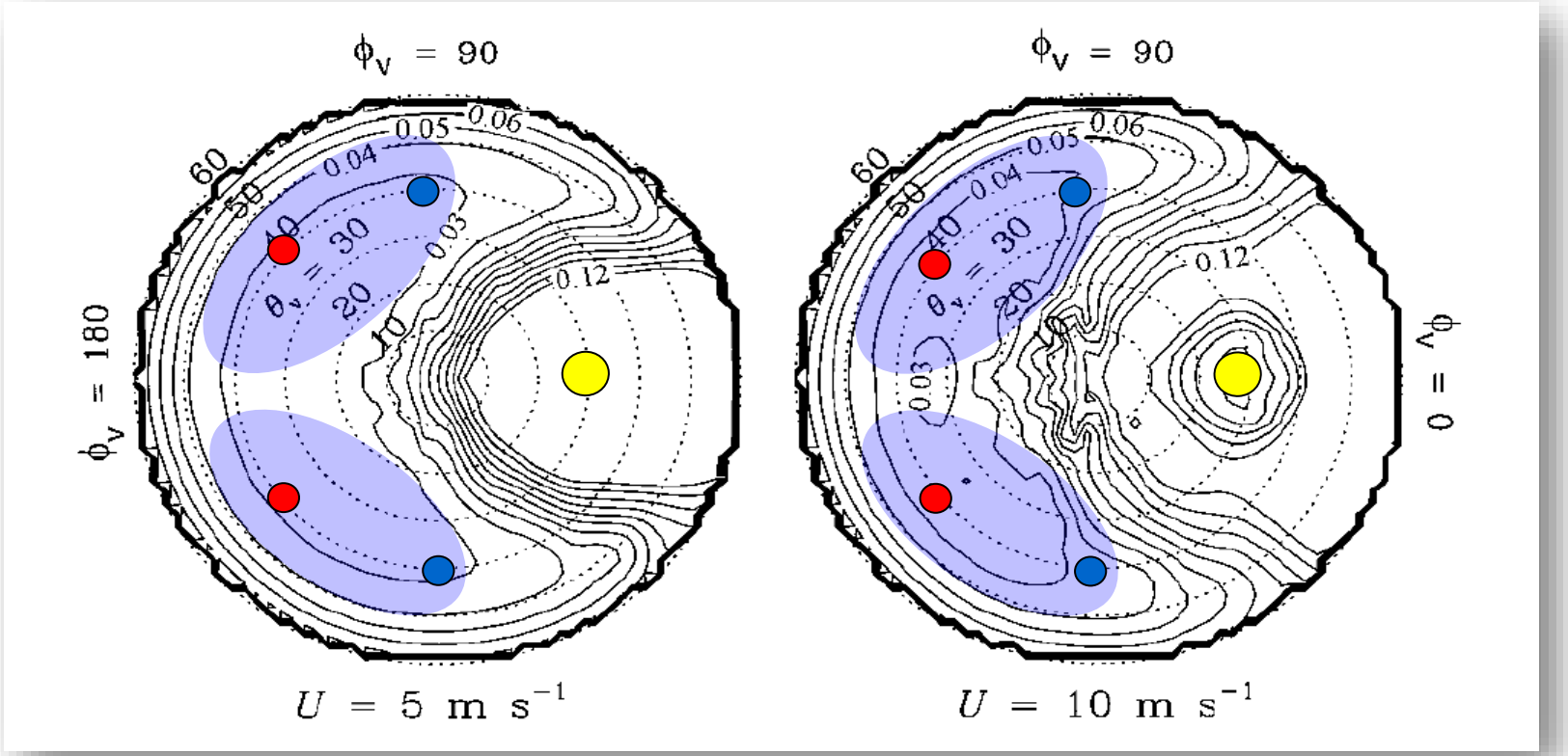

Distribution of ρ -factors

C.Mobley, Estimation of remote-sensing reflectance from above surface measurements. Applied Optics, 38: 7442-7455,1999.

Which relative azimuth angle?

Mobley (1999) suggested a viewing angle $\theta = 40°$ and a relative azimuth $\phi = 135°$ as the most appropriate to minimize sun glint perturbations in above-water radiometry.
This recommendation is fully supported by the lower and more stable values of modelled ρ-factors determined for diverse sun zeniths and sea states with ϕ=135°.

However, when using $\phi = 135°$, the L_T radiometer would generally look at the sea close to the deployment structure or at its shadow. Because of this, the selection of the relative azimuth angle needs to trade-off between a measurement geometry minimizing glint effects and that minimizing structure perturbations: ϕ = 90° is considered a viable solution.

A relevant element, often overlooked in above-water radiometry, is *the need to correct $L_w(\theta, \theta_0, \phi, \lambda)$ for the non-nadir view of the L_T sensor* due to the non-isotropic distribution of the in-water radiance. This correction implies assumptions on the bidirectional reflectance properties of the water and the application of consistent modelling solutions.
This need should discourage the adoption of diverse values of ϕ for operational measurements.
In fact, correction factors determined for diverse measurement geometries would be very likely affected by different uncertainties, which would naturally lead to potential intra-measurement inconsistencies.

Which viewing angle ?

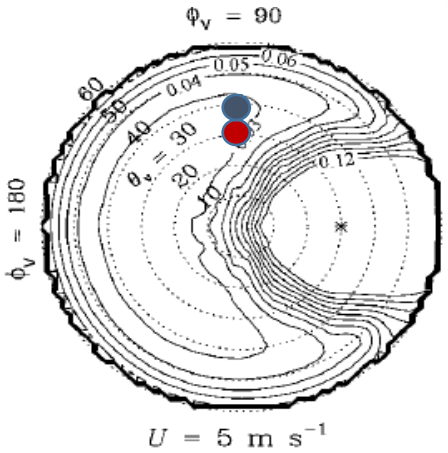

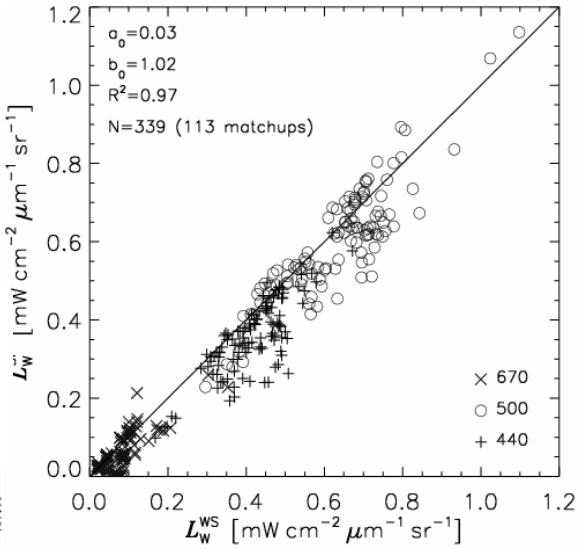

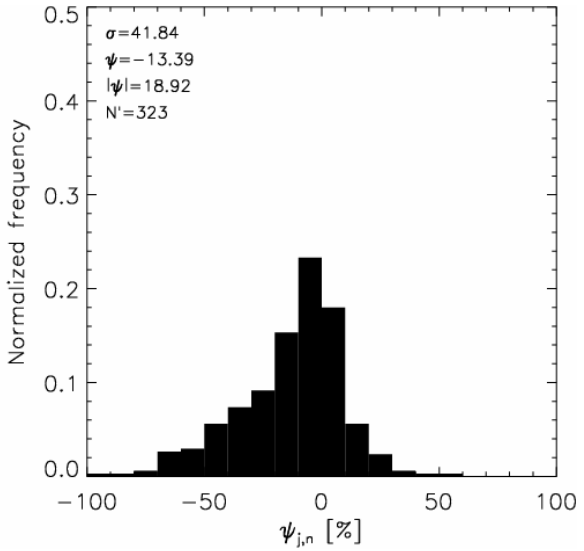

$\theta = 30^0$
$\phi = 90^0$
$\rho = 0.030$

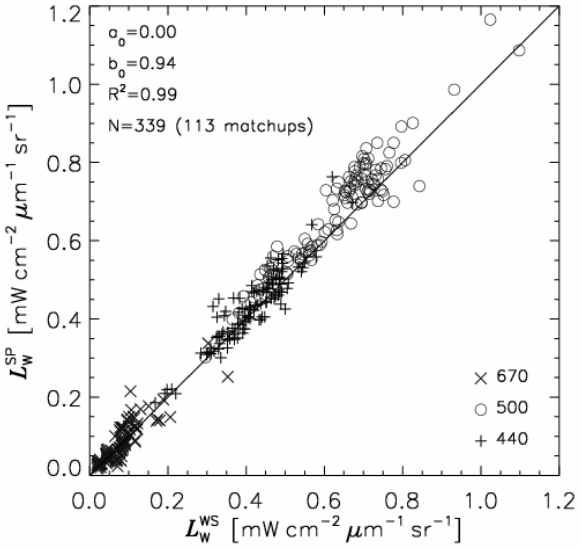

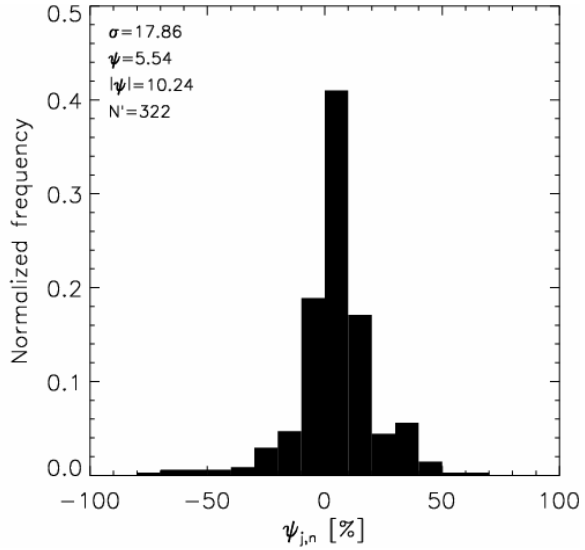

$\theta = 40^0$
$\phi = 90^0$
$\rho = 0.028$

Comparison results for θ=30° indicate a larger spread with respect to θ=40°, likely suggested by a higher dependence on sea state.

G. Zibordi, S. Hooker, J-F. Berthon, D. D'Alimonte. Autonomous above water radiance measurements from stable platforms. *Journal of Atmospheric and Oceanic Technology, 19: 808-819, 2002.*

Which ρ ?

Mobley 1999: ρ determined at 550 nm using the Hydrolight radiative transfer code by modelling the effects of sea state as a function of wind speed using Cox-Munk surfaces . The sky radiance distribution is determined from an irradiance model and experimental sky radiance patterns by neglecting polarization effects, but implicitly including multiple scattering and aerosol effects.

Mobley 2015: ρ determined at 550 nm accounting for the wave height and slope variance, in addition to the reflection and transmission processes involving polarized radiance at the water surface. Opposite to previous surface reflectance factors, the new ones are determined for a clear purely molecular sky (*i.e.,* Rayleigh) applying a single scattering analytic radiance model. Consequently, this specific ideal case can be considered as *representative of extreme polarization effects because of the absence of depolarization contributions from aerosols*.

Zhang et al. 2017: ρ determined for a number of spectral wavelengths using a vector radiative transfer code by modelling the effects of sea state as a function of wind speed using Cox-Munk surfaces and fully *accounting for polarization effects as a function of aerosols load. The values of ρ are separately determined for the direct sun and sky radiance.*

Tristan 2023: ρ determined for a number of spectral wavelengths using a vector radiative transfer code by modelling the effects of sea state as a function of wind speed using Cox-Munk surfaces and fully *accounting for polarization effects as a function of aerosols type and load. The values of ρ are separately provided for the direct sun and sky radiance*.

Polarization and wind – sun zenith dependence

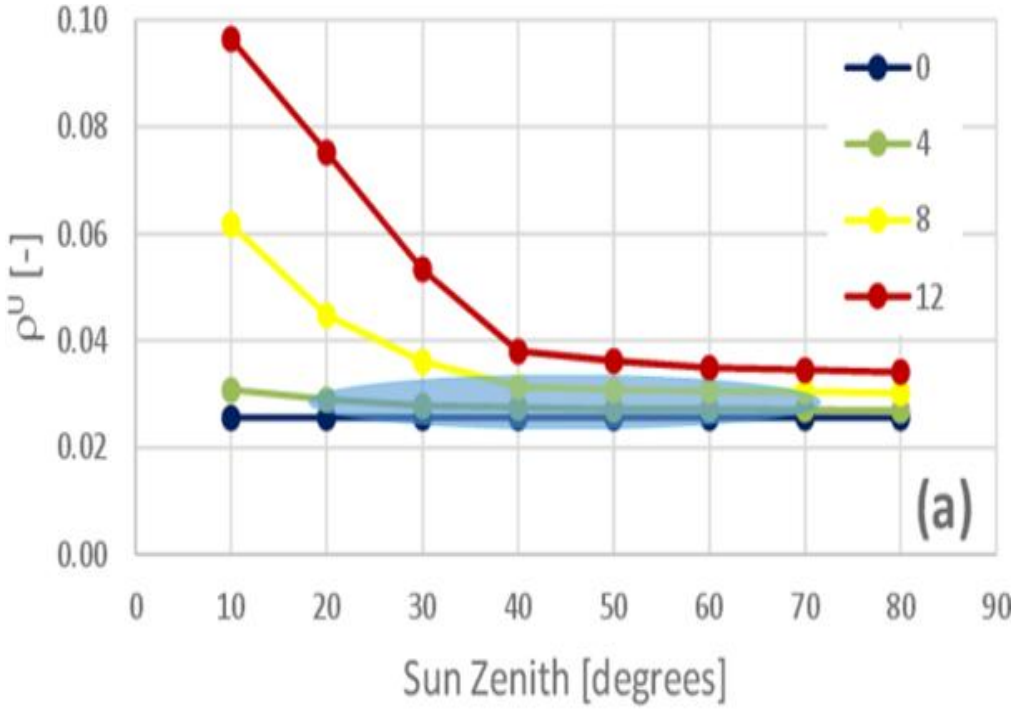

Mobley, C. D. (1999). Estimation of the remote-sensing reflectance from above-surface measurements. *Applied optics*, *38*(36), 7442-7455.

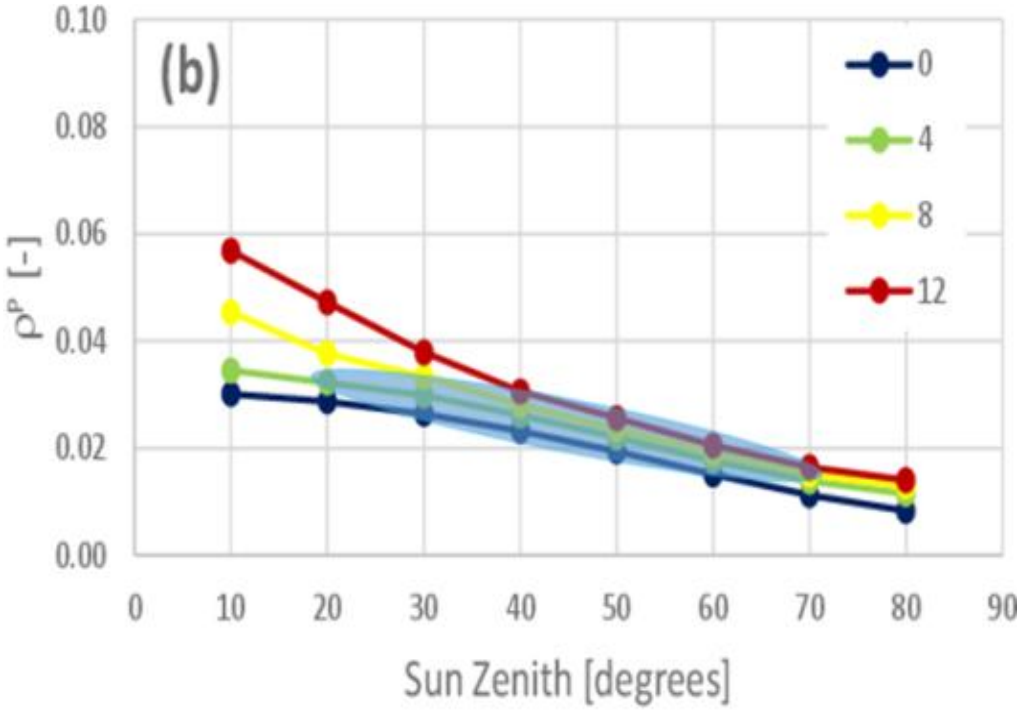

Mobley, C. D. (2015). Polarized reflectance and transmittance properties of windblown sea surfaces. *Applied optics*, *54*(15), 4828-4849.

The ρ-factors proposed by Mobley in 1999 and those in 2015, exhibit differences more marked for low and high sun zenith angles.

Assessment of above-water L_W with ρ^U

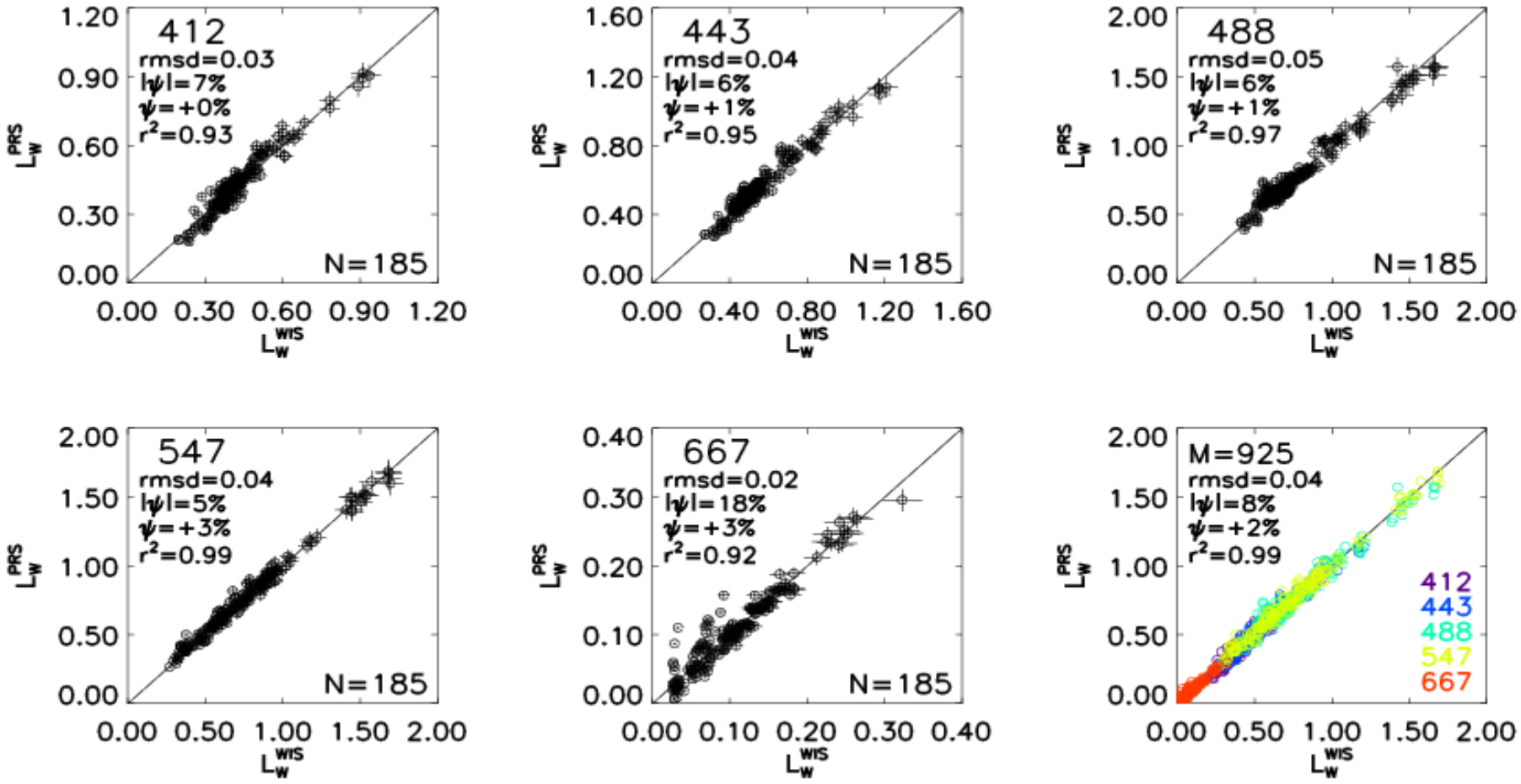

G. Zibordi. An experimental evaluation of theoretical sea surface reflectance factors relevant to above-water radiometry. Optics Express, 2016.

Assessment of above-water L_W with ρ^P

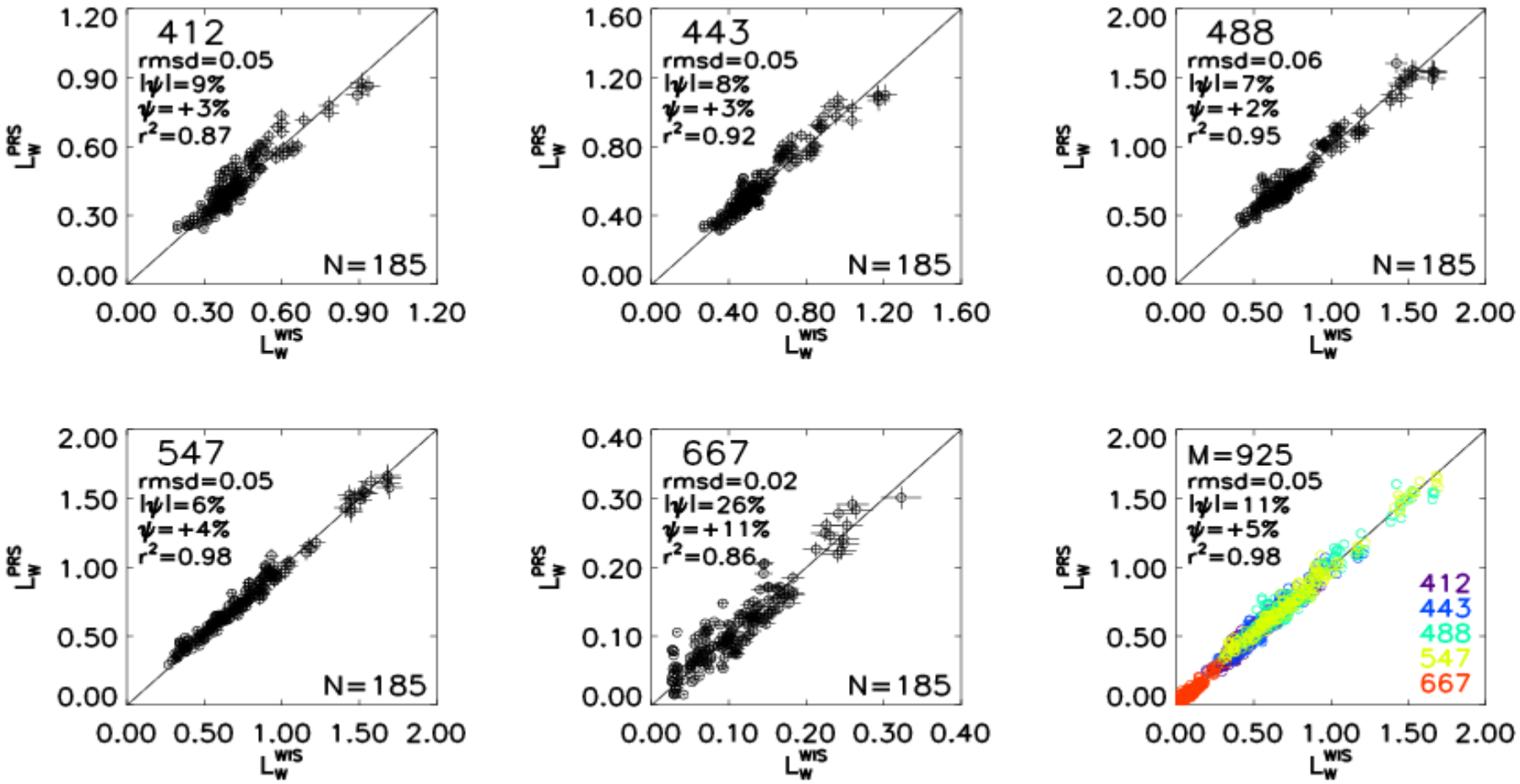

G. Zibordi. An experimental evaluation of theoretical sea surface reflectance factors relevant to above-water radiometry. Optics Express, 2016.

In-water radiance distribution

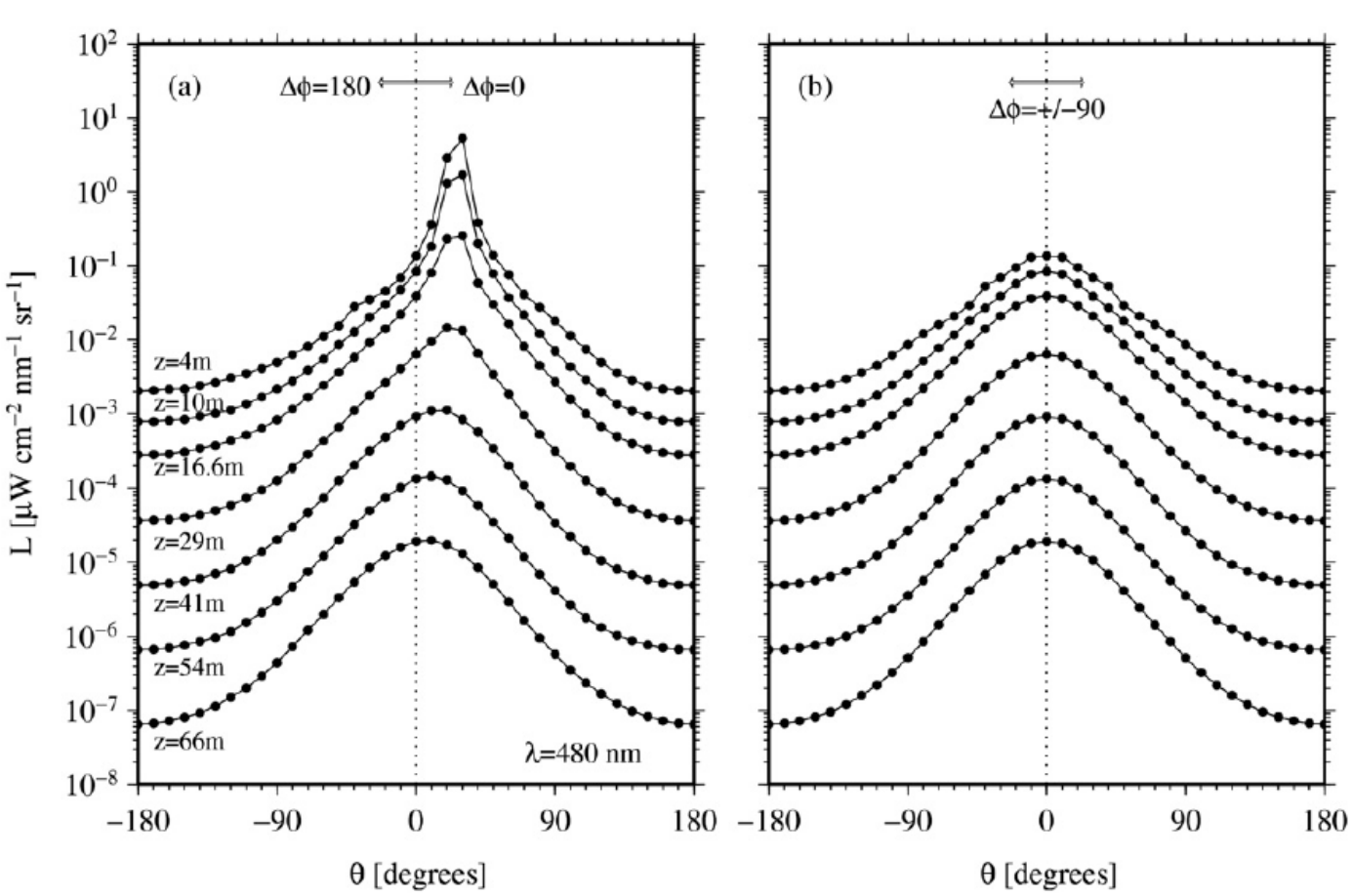

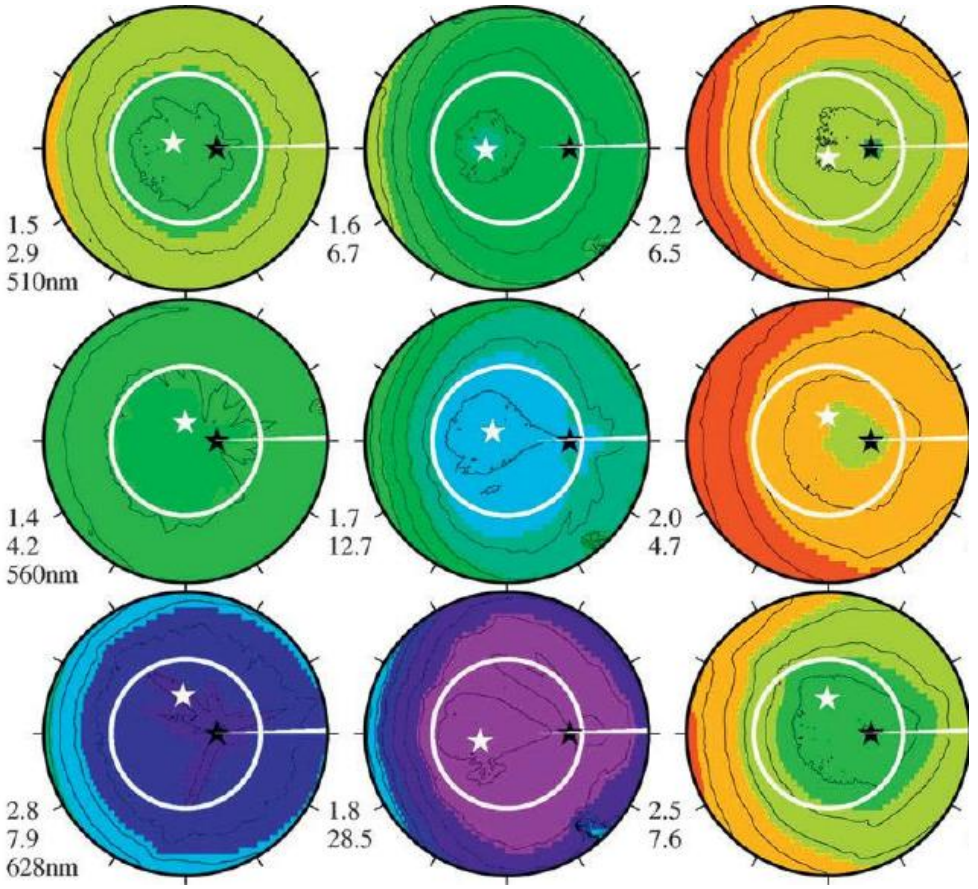

The in-water radiance distribution is non isotropic !

Tyler, J. E. (1960). Radiance distribution as a function of depth in an underwater environment. Bull. Scripps Iinst. Oceanogr., 7, 363-412.

Antoine, D., Morel, A., Leymarie, E., Houyou, A., Gentili, B., Victori, S., ... & Henry, P. (2013). Underwater radiance distributions measured with miniaturized multispectral radiance cameras. Journal of Atmospheric and Oceanic Technology, 30(1), 74-95.

Chla-based brdf correction

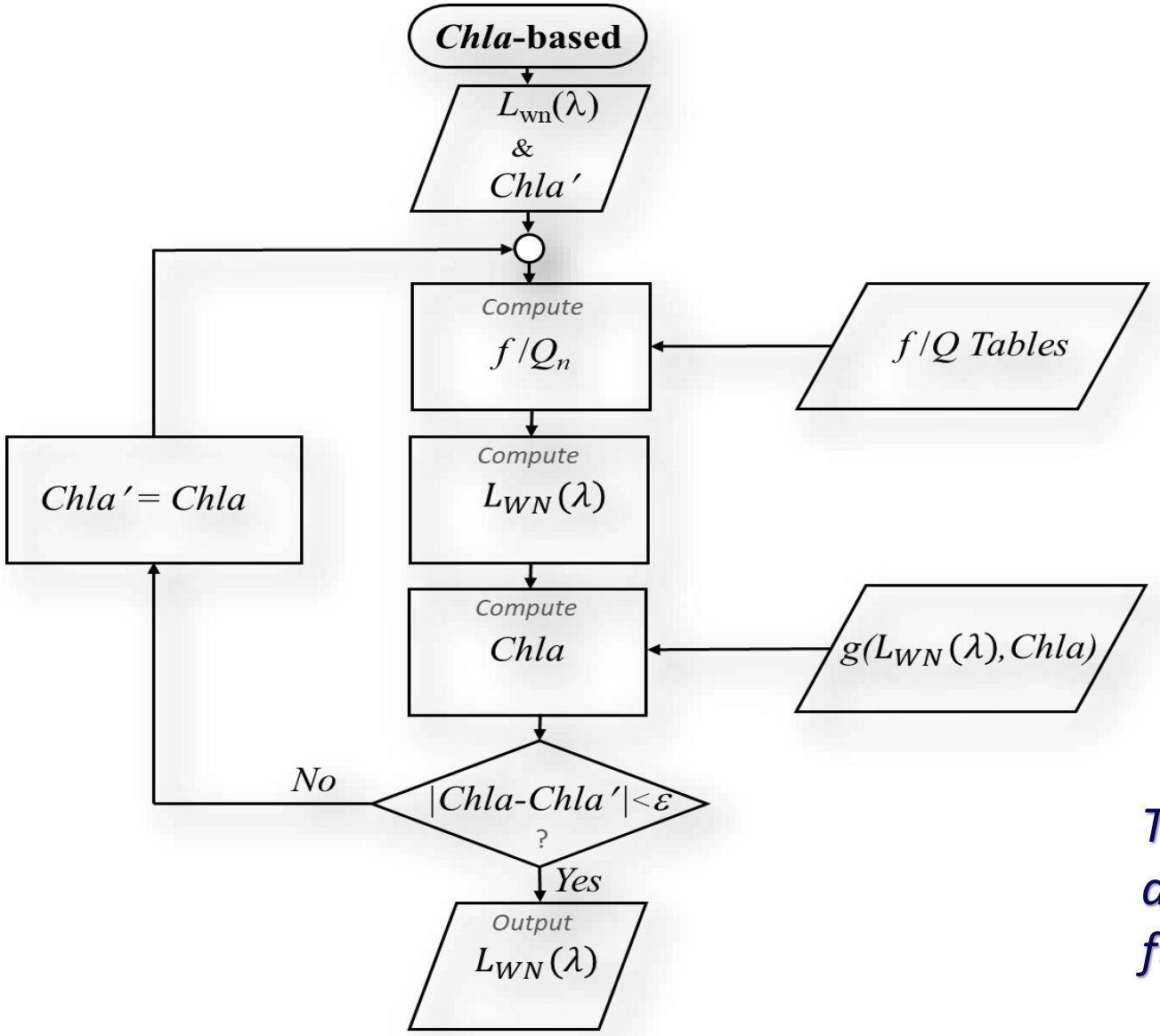

Removal of the viewing angle dependence

$$L_w(\lambda) = L_w(\theta,\varphi,\lambda)\frac{\Re_0}{\Re(\theta,W)}\frac{Q(\theta,\varphi,\theta_0,\lambda,\tau_a,IOP)}{Q_n(\theta_0,\lambda,\tau_a,IOP)}$$

$f(\theta_0,\lambda,\tau_a,IOP)$ missing because cancelling out

Basic correction for the illumination conditions

$$L_{wn}(\lambda) = \frac{L_w(\lambda)}{E_S(\lambda)}E_0(\lambda)$$

Removal of the sun-zenith dependence

$$L_{WN}(\lambda) = L_{wn}(\lambda)\frac{f(0,\lambda,\tau_a,IOP)}{Q_n(0,\lambda,\tau_a,IOP)}\left[\frac{f(\theta_0,\lambda,\tau_a,IOP)}{Q_n(\theta_0,\lambda,\tau_a,IOP)}\right]^{-1}$$

The f/Q_n factors, which account for anisotropy, are tabulated with IOPs solely expressed as function Chla (Morel et al., 2002)

Proposed for Chla dominated waters !

Morel, A., Antoine, D., & Gentili, B. (2002). Bidirectional reflectance of oceanic waters: accounting for Raman emission and varying particle scattering phase function. Applied Optics, 41(30), 6289-6306.

IOP-based brdf correction

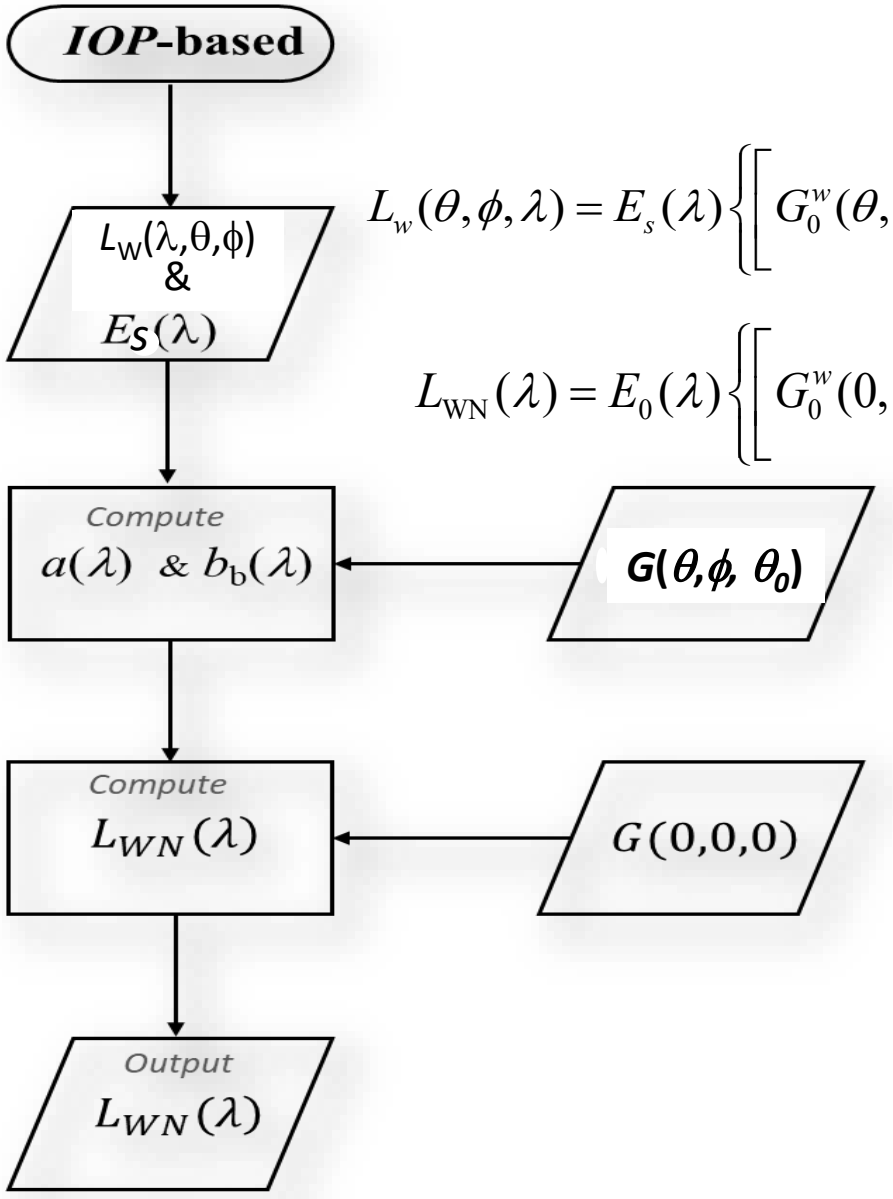

$$L_w(\theta,\phi,\lambda) = E_s(\lambda)\left\{\left[G_0^w(\theta,\phi,\theta_0) + G_1^w(\theta,\phi,\theta_0)\cdot\frac{b_{bw}(\lambda)}{k(\lambda)}\right]\cdot\frac{b_{bw}(\lambda)}{k(\lambda)} + \left[G_0^p(\theta,\phi,\theta_0) + G_1^P(\theta,\phi,\theta_0)\cdot\frac{b_{bp}(\lambda)}{k(\lambda)}\right]\cdot\frac{b_{bp}(\lambda)}{k(\lambda)}\right\}$$

$$L_{WN}(\lambda) = E_0(\lambda)\left\{\left[G_0^w(0,0,0) + G_1^w(0,0,0)\cdot\frac{b_{bw}(\lambda)}{\kappa(\lambda)}\right]\cdot\frac{b_{bw}(\lambda)}{\kappa(\lambda)} + \left[G_0^p(0,0,0) + G_1^P(0,0,0)\cdot\frac{b_{bp}(\lambda)}{\kappa(\lambda)}\right]\cdot\frac{b_{bp}(\lambda)}{\kappa(\lambda)}\right\}.$$

See Lee et al. 2004 for model details

$K(\lambda)=a(\lambda)+b_b(\lambda)$

The G factors are tabulated and express dependence on geometry (Lee et al., 2011).

Tentatively proposed for any water type

Lee, Z., Carder, K. L., & Du, K. (2004). Effects of molecular and particle scatterings on the model parameter for remote-sensing reflectance. Applied Optics, 43(25), 4957-4964.

Lee, Z. P., Du, K., Voss, K. J., Zibordi, G., Lubac, B., Arnone, R., & Weidemann, A. (2011). An inherent-optical-property-centered approach to correct the angular effects in water-leaving radiance. Applied Optics, 50(19), 3155-3167.

Corrections for bidirectional effects

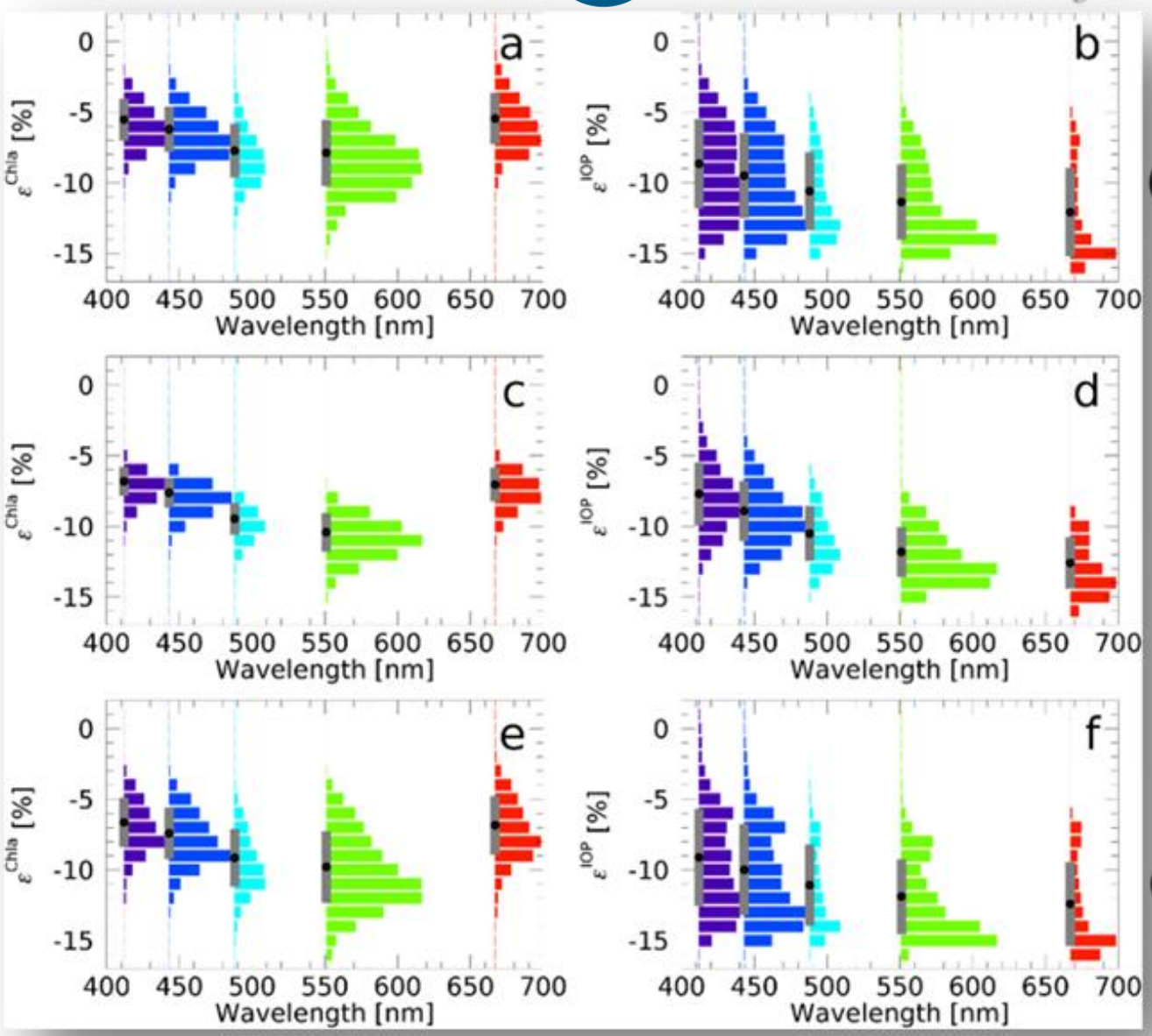

AAOT
(Adriatic Sea)

Gloria
(Black Sea)

Gustaf
Dalen
(Baltic Sea)

Talone, M., Zibordi, G., & Lee, Z. (2018). Correction for the non-nadir viewing geometry of AERONET-OC above water radiometry data: An estimate of uncertainties. Optics Express, 26(10), A541-A561.

Corrections for bidirectional effects

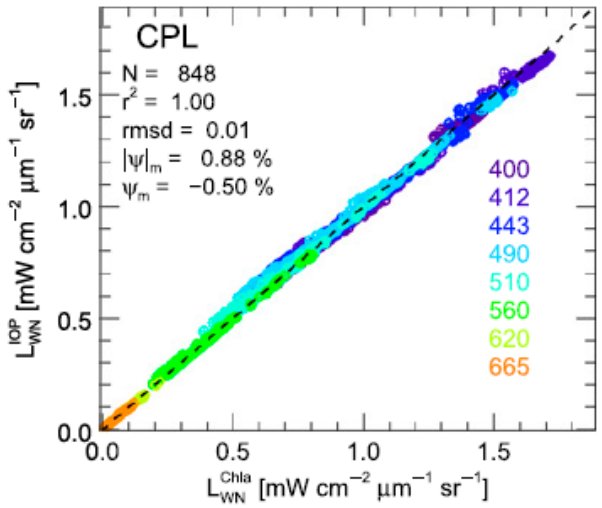

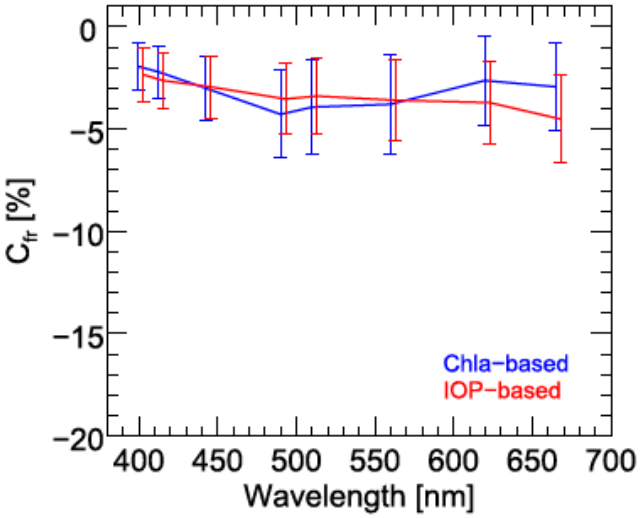

Shows convergence over Case-1 waters for which both corrections are ideally applicable

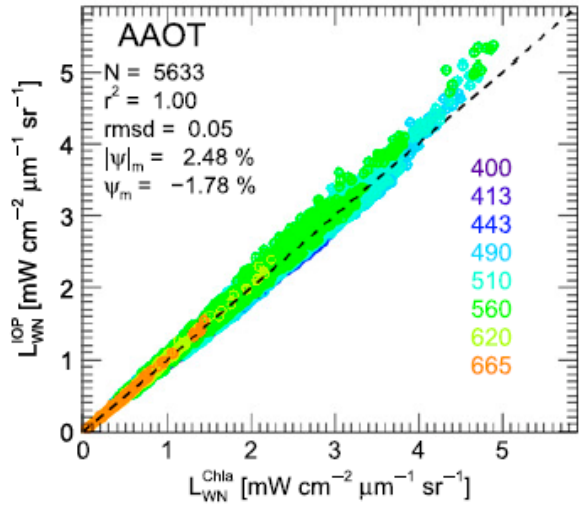

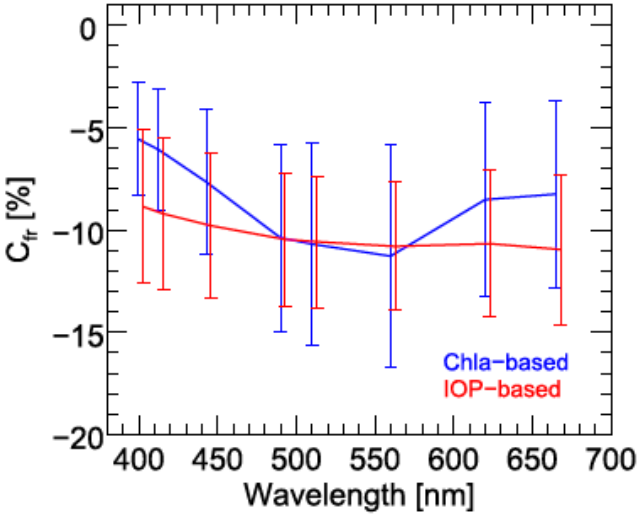

As expected, does not show systematic convergence over optically complex waters

Talone, M., Zibordi, G., & Lee, Z. (2018). Correction for the non-nadir viewing geometry of AERONET-OC above water radiometry data: An estimate of uncertainties. *Optics Express*, *26*(10), A541-A561.

Uncertainties affecting off-nadir corrections

Optical Floating System

Sampled Regions

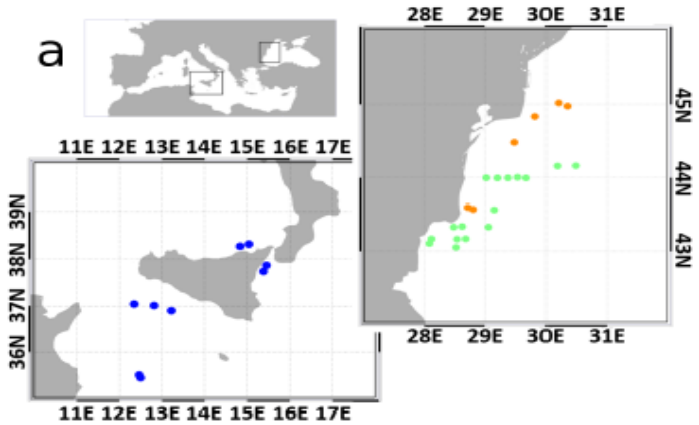

Sampled Spectra

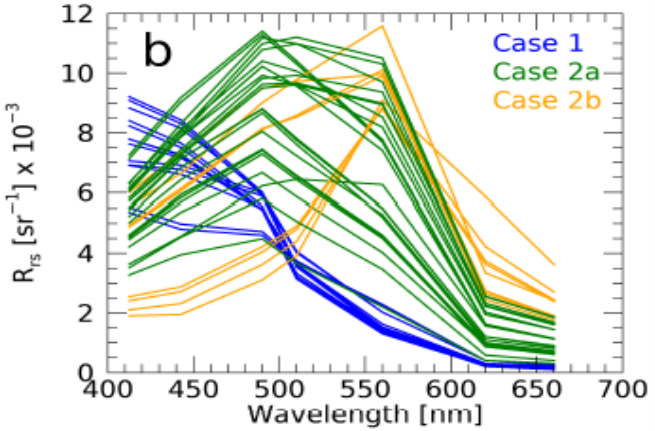

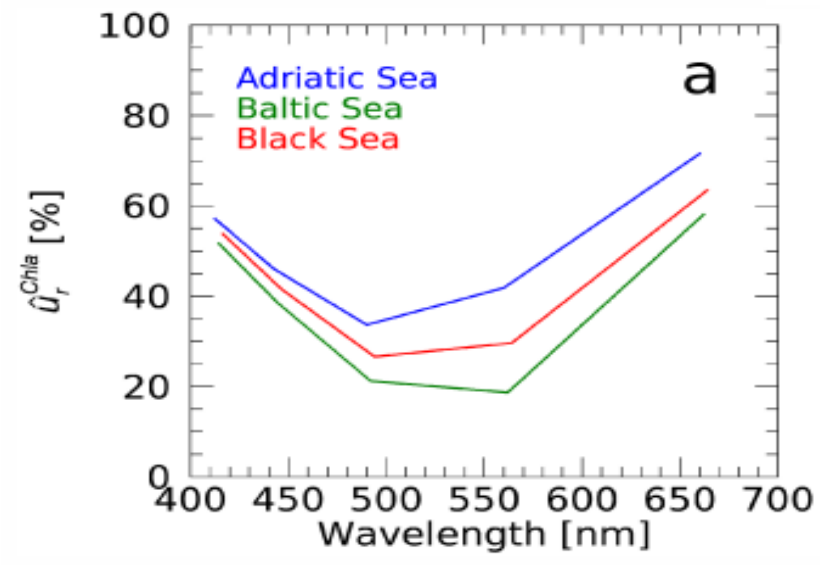

Chla-Based Approach

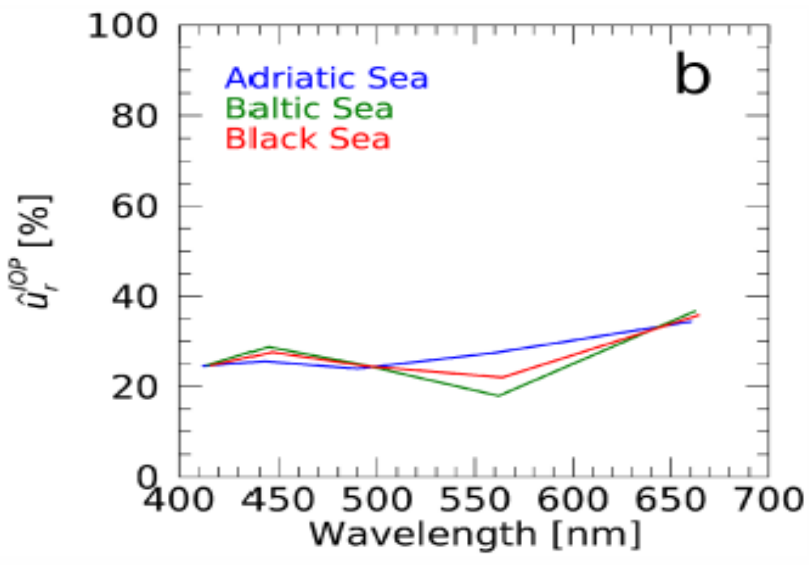

IOP-Based Approach

M. Talone, G. Zibordi and Z. Lee., Correction for the non-nadir viewing geometry of AERONET-OC above-water radiometry data: an estimate of uncertainties. Optics Express, 2018

Sample L_{WN} spectra

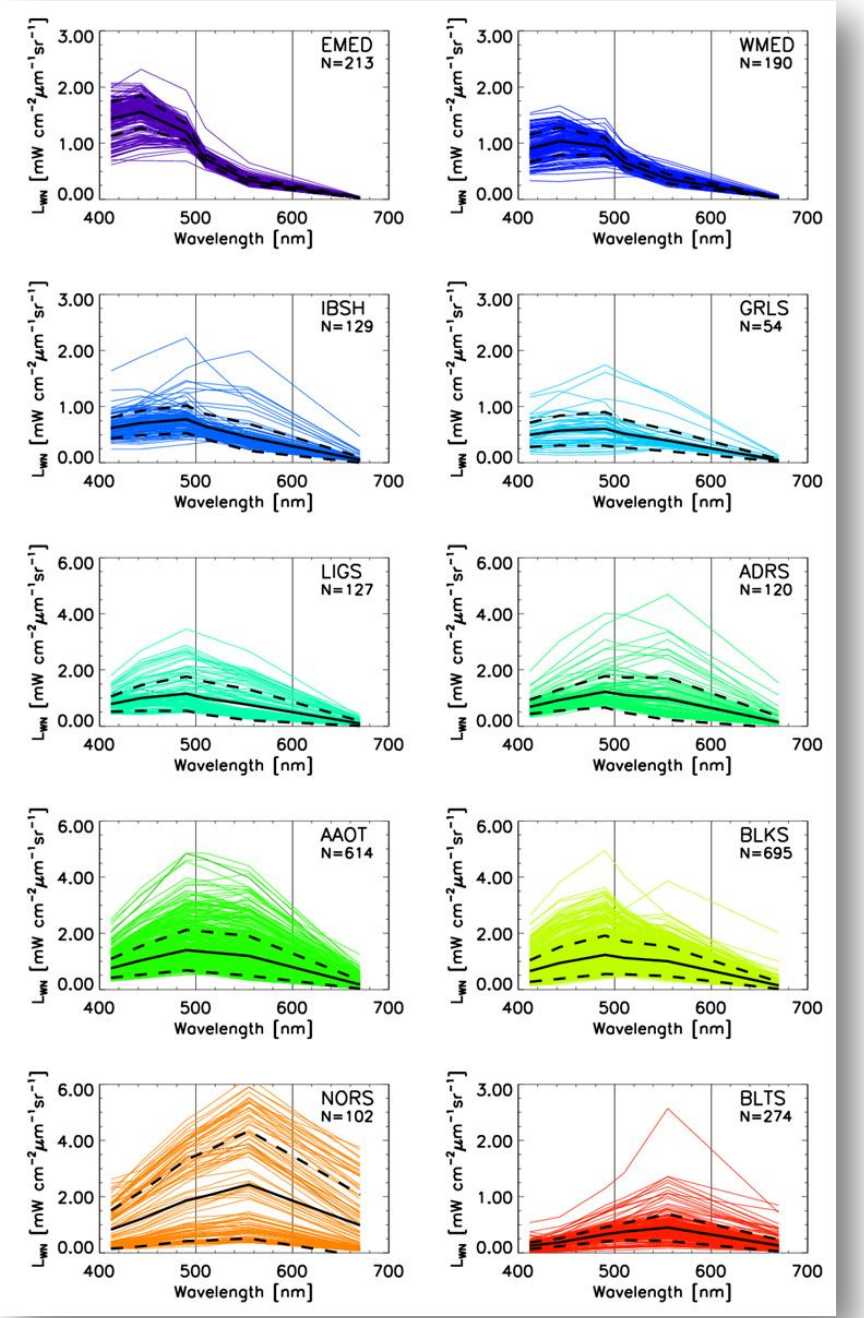

Case1 waters: optical properties solely determined by phytoplankton and its degradation components.

Absorption coefficients of diverse optically significant constituents

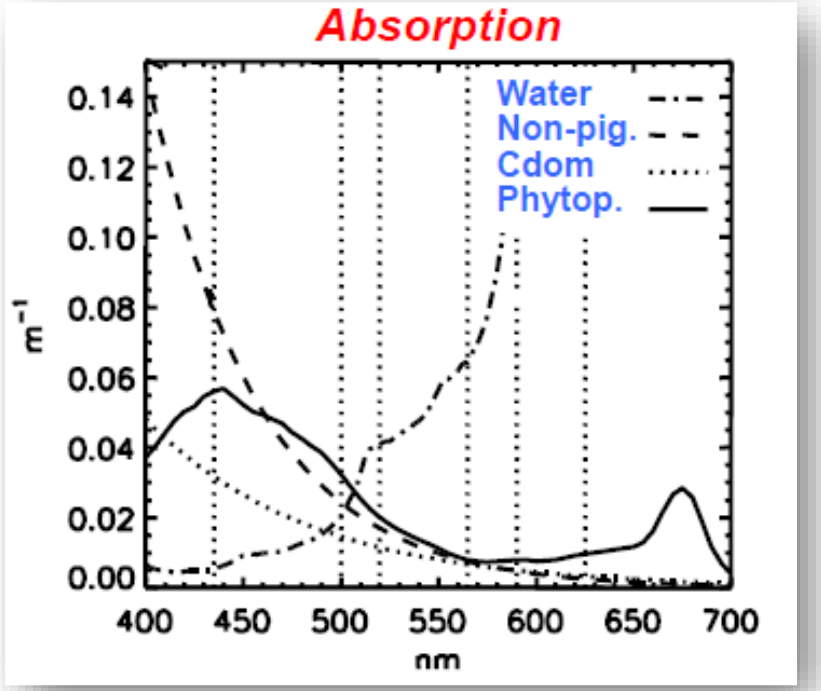

Optically complex waters: optical properties determined by uncorrelated concentrations of phytoplankton, sediment and coloured dissolved organic matter.

Optically complex waters: optical properties heavily dominated by coloured dissolved organic matter.

Assessment of instruments performance via inter-comparisons

Comparison of L_{WN} data from a 12-channel and a 9-channel AERONET-OC instruments for equivalent measurement conditions

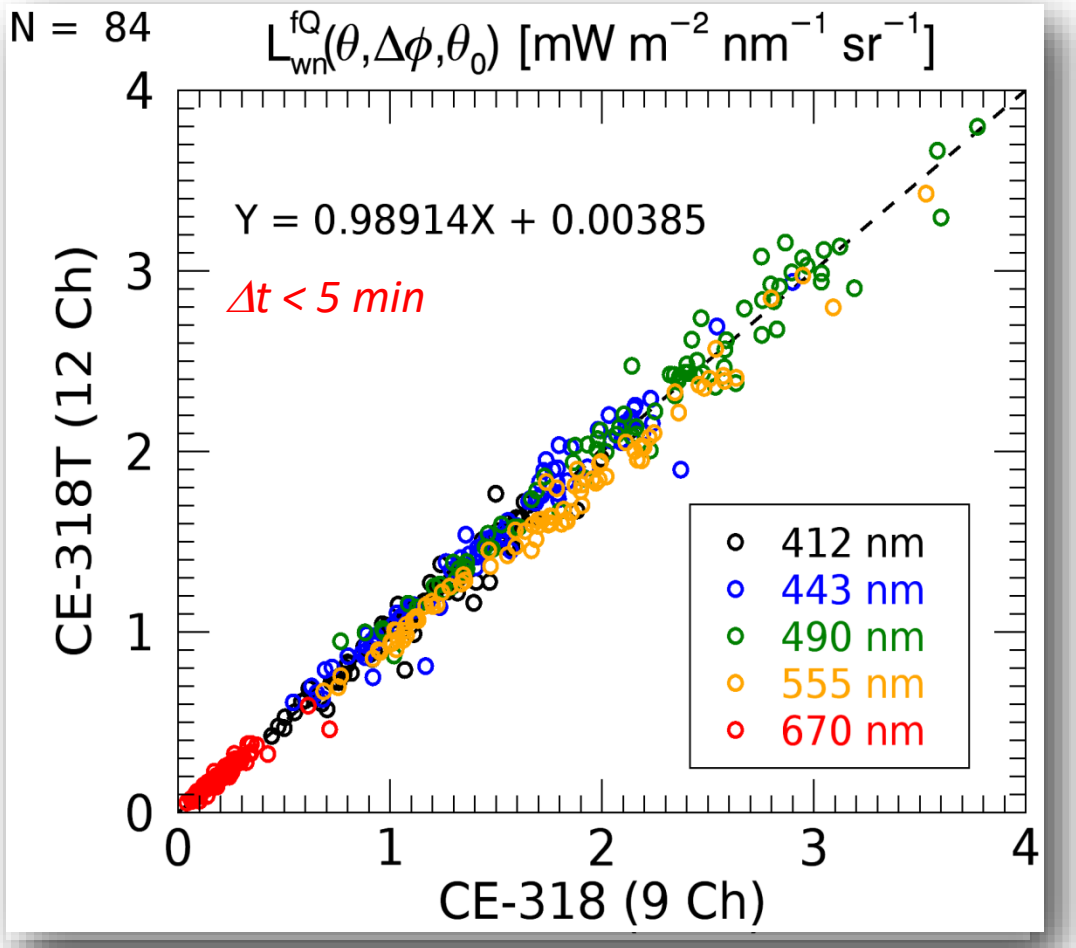

Zibordi, G., Holben, B. N., Talone, M., D'Alimonte, D., Slutsker, I., Giles, D. M., & Sorokin, M. G. (2021). Advances in the Ocean Color component of the Aerosol Robotic Network (AERONET-OC). Journal of Atmospheric and Oceanic Technology, 38(4), 725-746.

Alternative above-water measurement approaches

The general method discussed here relies on the application of calibrated radiometers allowing for absolute spectral measurements of the total radiance from the sea surface $L_T(\theta,\phi,\lambda)$ (which includes contributions from $L_w(\lambda)$, sky–glitter, and sun–glint) and of the sky $L_i(\theta',\phi,\lambda)$ (i.e., sky radiance).

The downward irradiance $E_s(\lambda)$ is a desirable quantity for the minimization of changes in illumination during measurements and to compute the remote sensing reflectance $R_{RS}(\lambda)$.

Alternative methods such as those relying on plaques (Carder and Steward 1985,) or polarizers (Fougnie et al. 1999), are challenged by non-ideal field implementations (in the case of plaques) and by the application of comprehensive radiative transfer models (in the case of polarizers), which may affect the accurate quantification of products uncertainties.

Also alternative data processing solutions proposed in the literature mostly centered on the optimization of the sky-glint removal (i.e., the minimization of any residual sky radiance affecting $L_w(\lambda)$: Lee et al. 1997, Gould et al. 2000, Ruddick et al., 2006, Simis and Olsson 2013, Kutser et al. 2013, Groetsch et al. 2017), have not shown clear effectiveness on data collected during clear sky.

End

In-water radiometry

Historical dates

1920s: First successful measurements
1960s: Accurate absolute calibrations
1990s: Methods assessment
2000s: Comprehensive uncertainty analysis

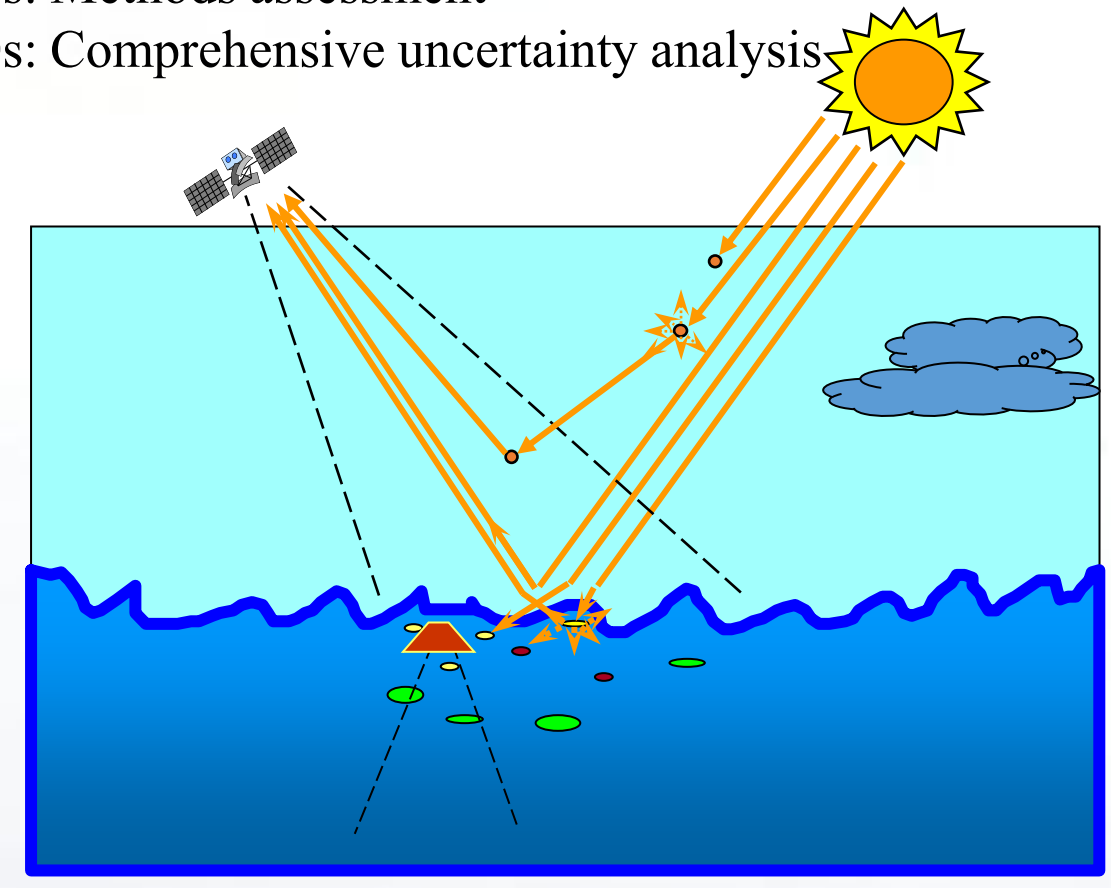

Advantages

1. Produces comprehensive (continuous or fixed depths) profiles of radiometric quantities
2. Open to the quantification of several radiometric quantities (i.e., L_w, E_d, E_u)
3. Upward radiometric quantities are almost not affected by wave perturbations

Drawbacks

1. Long-term deployments can be very sensitive to bio-fouling
2. Sensitive to coastal water optical stratifications
3. Requires corrections for self-shading

In-water radiometry

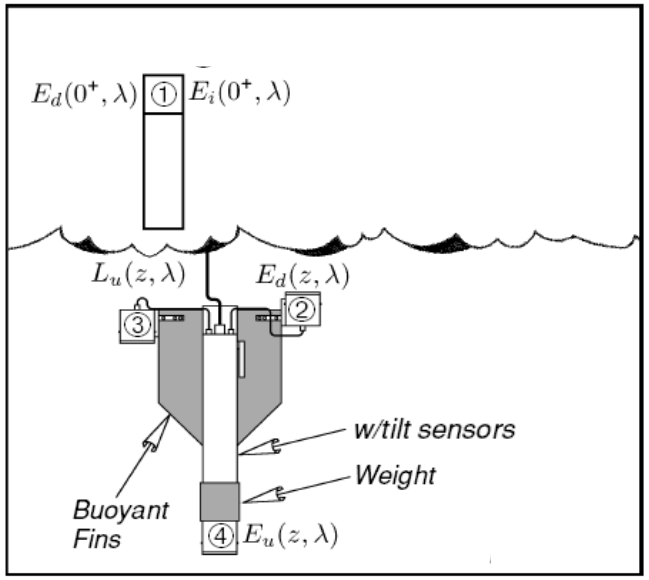

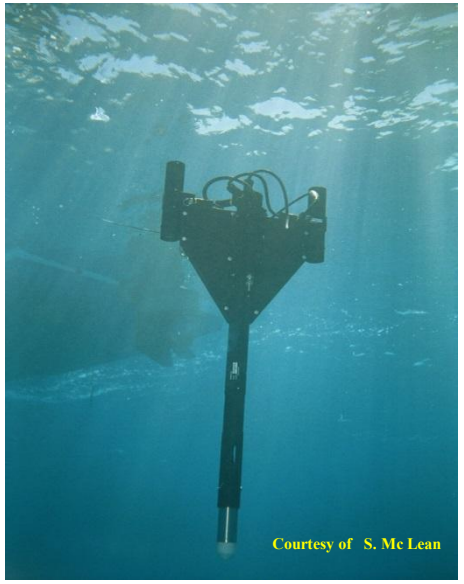

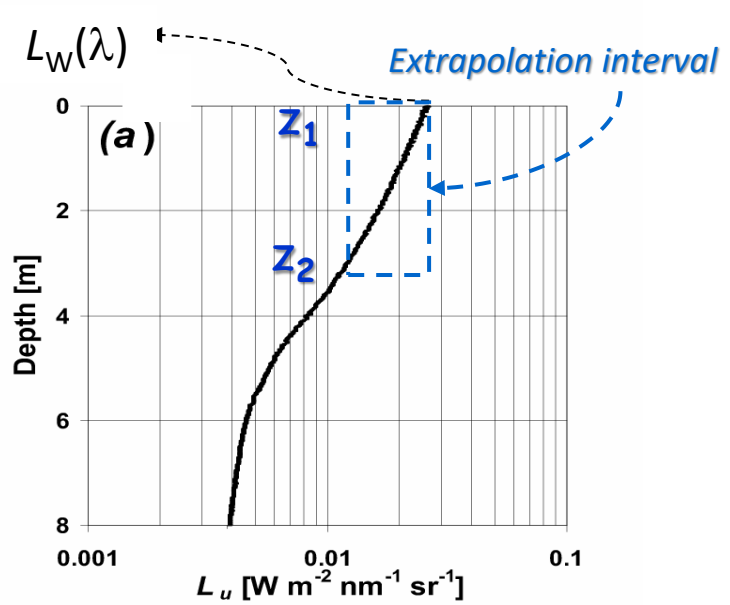

$$L_u(z,\lambda,t_0) = \frac{L_u(z,\lambda,t)}{E_d(0^+,\lambda,t)} E_d(0^+,\lambda,t_0)$$

$$L_u(0^-,\lambda) = L_u(z_0,\lambda,t_0) / e^{-K_d(z_1,z_2,\lambda)z_0}\, C_{ss}(\lambda,a,r,\theta_0)$$

$$L_W(\lambda) = \frac{t_{aw}(\lambda)}{n_w^2(\lambda)} L_u(0^-,\lambda)$$

$$L_{WN}(\lambda) = L_W(\lambda) \frac{E_0(\lambda)}{E_d(0^+,\lambda)} C_{f/Q}(\lambda,\theta_0,\tau,IOP)$$

Smith, R. C., & Baker, K. S. (1984). The analysis of ocean optical data. In *Ocean optics VII* (Vol. 489, pp. 119-126). SPIE.

Lewis, M. R., Hebert, D., Harrison, W. G., Platt, T., & Oakey, N. S. (1986). Vertical nitrate fluxes in the oligotrophic ocean. *Science*, *234*(4778), 870-873.

Waters, K. J., Smith, R. C., & Lewis, M. R. (1990). Avoiding ship-induced light-field perturbation in the determination of oceanic optical properties. *Oceanography*, *3*(2), 18-21.

Introduction to above-water radiometry

Outline

- Definition of radiometric quantities
  - Radiance and irradiance, L_W, L_{WN}, R_{RS}
- Optical radiometers
  - Irradiance sensors (angular response)
  - Radiance sensors (field of view)
  - Multi-spectral *vs* hyper-spectral
- Principles of above-water radiometry
- The ρ-factor
  - Theoretical determination
  - Sun zenith and wind speed dependence
  - Spectral dependence
- Data reduction and processing
  - Data reduction and L_W determination
  - Viewing angle and BRDF corrections
- Inter-comparisons supporting QA

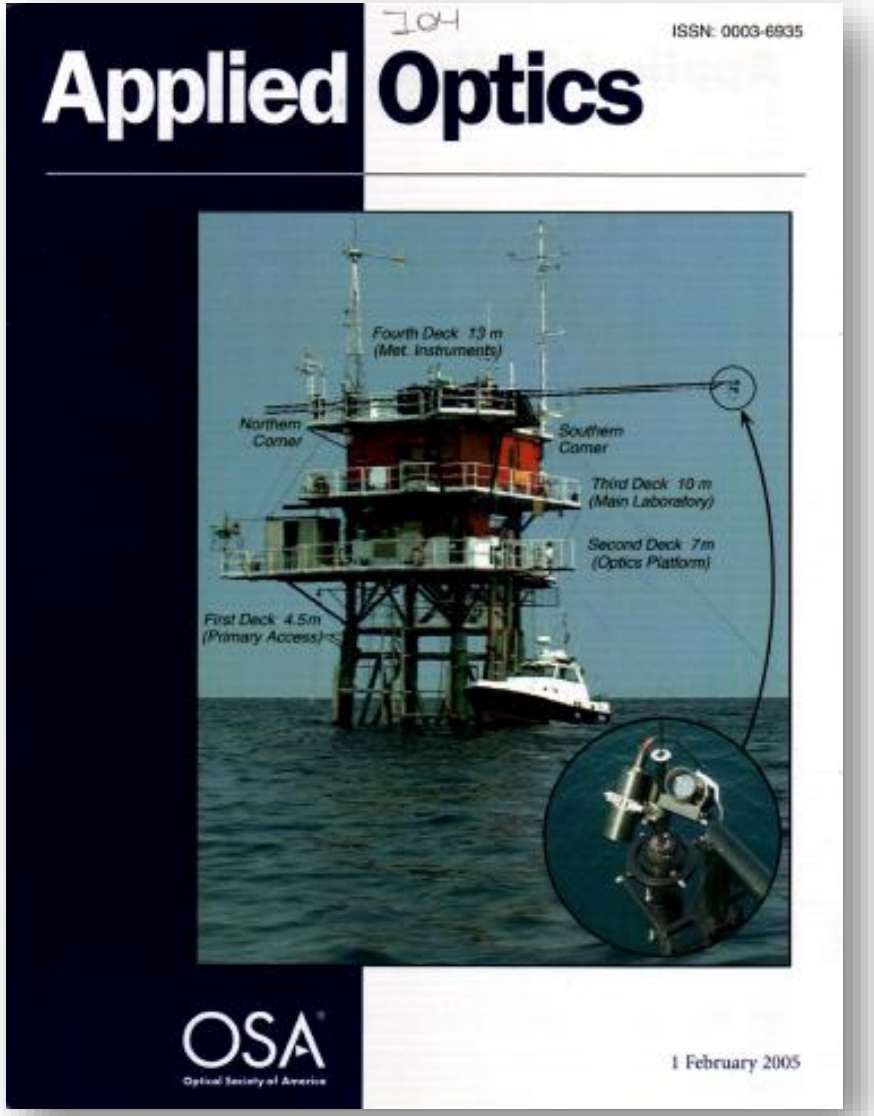

Radiometric quantities and units

Radiometry is the science dealing with the properties of the electromagnetic radiation.
In the specific case of ocean colour, radiometry focusses on spectral radiance and plane irradiance in the visible and near-infrared regions of the spectrum (tentatively 400-700 nm).

Radiometric Quantity	Symbol	Units (mks)
Radiant energy	Q	J
Radiant flux (power)	Φ	W
Irradiance 	E	$W\,m^{-2}$
Radiance 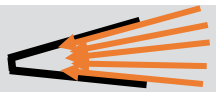	L	$W\,m^{-2}\,sr^{-1}$

These units are often expressed in "per unit wavelength"